

Studies of meteor head echo signatures at polar latitudes

Kumulative Dissertation
zur
Erlangung des akademischen Grades
doctor rerum naturalium (Dr. rer. nat.)
der Mathematisch-Naturwissenschaftlichen Fakultät
der Universität Rostock



vorgelegt von
Carsten Schult, geb. am 06.07.1987 in Rostock, Deutschland
Rostock, 16. Februar 2018

Betreuer: Prof. Dr. J. L. Chau
Leibniz-Institut für Atmosphärenphysik an der Universität Rostock

Gutachter: Prof. Dr. J. L. Chau
Leibniz-Institut für Atmosphärenphysik an der Universität Rostock
Prof. Dr. S. Close
Stanford University, Department of Aeronautics and Astronautics
Prof. Dr. M. Oppenheim
Center for Space Physics, Boston University

eingereicht am: 16. Februar 2018

verteidigt am: 10. August 2018

Abstract

Extraterrestrial particles entering the Earth's atmosphere with a sufficient amount of kinetic energy can be observed as meteors in a clear night or as meteor echoes by using radar observations. High power large aperture (HPLA) radars are able to detect the small plasma cloud that is formed around the meteoroid during the ablation process, which is called meteor head echo. In contrast to optical meteor observations, radar systems can measure independent of weather conditions as well as during day and night. On the other hand, only a few atmospheric HPLA radars exist world-wide and measurement time is expensive, making meteor head echo observations rare and limited in their duration. This thesis presents the first continuous meteor head echo observations over two years. Seasonal variations in the sporadic meteor background, dynamic masses and velocity distributions are studied. A comparison with an empirical meteor input function shows good agreement in the overall count rates, but larger deviations in the slow velocity regime. Furthermore, the distributions of the meteoroid source radiants have to be adjusted to fit the observation. This unique data set is also analyzed for the search of meteor showers. It is shown that a lot of meteoroid streams also contain particles with masses in order of one microgram. A first overview of a comparison with 105 optical meteors is presented. In addition, a meteor fireball, detected by a standard specular meteor radar, was studied with respect to the trajectory, orbital elements and a meteor ablation model. It is found that the corresponding meteoroid had to be at least three times heavier than it was stated in an earlier study.

Zusammenfassung

Extraterrestrische Teilchen verdampfen, bei einer ausreichenden Menge an kinetischer Energie, wenn sie auf die Erdatmosphäre treffen und können am Nachthimmel als Meteore beobachtet werden. Radarsysteme, die über eine große Apertur und Sendeleistung (high power large aperture, HPLA) verfügen, können, die kleinen Plasmawolken, welche um den verdampfenden Meteoroiden entstehen, beobachten. Das entsprechende Signal wird Meteor-Kopf-Echo genannt. Im Gegensatz zu optischen Beobachtungen von Meteoren, können Radarsysteme Messungen unabhängig von der Sonneneinstrahlung und den Wetterbedingungen durchführen, d.h. kontinuierliche Messung sind prinzipiell möglich. Da es nur wenige HPLA Atmosphären-Radarsysteme gibt, sind entsprechende Datensätze nur sehr beschränkt verfügbar. In dieser Arbeit werden die Ergebnisse der ersten quasi-kontinuierlichen Meteor-Kopf-Echobeobachtungen, über eine Dauer von über zwei Jahren, vorgestellt. Saisonale Variationen der sporadischen Quellen, dynamische Massen, sowie Geschwindigkeitsverteilungen werden untersucht. Ein Vergleich der erhobenen Daten, mit einem empirischen Modell des Meteoreintrags, zeigt eine gute Übereinstimmung in den Zählraten aber eine größere Abweichung bei kleinen Eintrittsgeschwindigkeiten. Des Weiteren muss die Verteilung der Meteorradianten im Modell angepasst werden, um mit den Beobachtungen übereinzustimmen. Der Datensatz wurde ebenfalls genutzt um Meteorschauer zu untersuchen. Dabei wird gezeigt, dass viele bekannte Meteorschauer auch Teilchen im Mikrogrammbereich enthalten. Ergänzt wurden die Messungen, über einen begrenzten Zeitraum, durch optische Kamerasysteme. Ein erster Vergleich mit 105 optisch beobachteten Meteoren konnte dadurch realisiert werden. Zudem wurde für einen Feuerball, beobachtet mit einem Meteorradar, eine detaillierte Analyse der Trajektorie vorgenommen und der Ablationsprozess mittels eines Modells untersucht. Hierbei wurde eine größere Eintrittsmasse ermittelt als andere Studien vorher abgeschätzt hatten.

Contents

Abstract	iii
Zusammenfassung	iv
1 Introduction	1
2 General overview of the characteristics of meteors	3
2.1 Ablation of meteoroids	3
2.2 Sources of meteoroids	5
2.3 Radar meteor echoes	7
3 Objectives of the thesis	10
4 Meteor-head echo observations using MAARSY	11
5 Radar observation of the Maribo fireball	14
6 Quasi-continuous meteor head echo survey	17
7 Simultaneous radar and optical meteor measurements	21
8 Meteor head echo shower survey with MAARSY	24
9 Summary and outlook	29
Bibliography	31
Appendix A Schult et al. (2013)	41
Appendix B Schult et al. (2015)	42
Appendix C Schult et al. (2017)	43
Appendix D Brown et al. (2017)	44
Appendix E Schult et al. (2018)	45
Appendix F Meteor head echo data analysis	46

Contents

Acknowledgements	51
Curriculum Vitae	52

Chapter 1 Introduction

The term meteor refers to the light emitted by fast extraterrestrial particles ablating in the Earth's atmosphere. If the event is extremely bright or attended with explosions it is also called fireball or bolide (*McKinley, 1961*). The ablating particle itself is called meteoroid. If parts of a meteoroid survive the flight through the atmosphere, the corresponding fragments are known as meteorites. From meteorite finds and spectral analysis of meteor trails it was found that the majority of meteoroids have a rocky compositions (84-95% chondritic, minerals with main components of Oxygen, Silicon, Magnesium, Sodium, Iron etc.) (*Ceplecha et al., 1998*). The smaller part refers to iron meteorites or achondrites.

The sizes of meteoroids vary from small dust grains to heavy objects of several tonnes. In general the meteoroid mass influx on Earth is very uncertain and differs by orders of magnitudes using different observation methods, ranging from 5 to 300 tonnes per day (*Plane, 2012*). That smaller particles are much more frequent than larger ones is beyond debate. Therefore the detection rate strongly depends on the sensitivity of the observation technique. *Drolshagen et al. (2017)* combined several observation techniques to get an overview of incoming particles in the range from $10^{-21}kg$ to $10^{12}kg$. The occurrence rate for meteoroids with masses in the order of one kilogram or higher is about one hundred thousand per year. For meteoroids of about one milligram or higher the count rate increases to the order of ten billions.

The lower limit for the meteoroids entry velocities is given by the Earth's gravity and the corresponding escape velocity of 11.2 km/s. The upper limit is reached at the Earth's perihelion, where the speed of the meteoroids and the Earth can add up to 72.8 km/s. Note, that the theoretical maximum is related to particles bound to the solar system (parabolic limit) (*Ceplecha et al., 1998*). The velocity distribution within these limits of particles entering the Earth atmosphere is still under debate and is also correlated to the meteoroid mass influx (e.g., *Carrillo-Sanchez et al., 2015; Janches et al., 2017; Williams et al., 2017*).

There exist several possibilities to study the meteoroid environment of the Earth. The most intuitive one is the optical observation of the light emitted by the meteor during the ablation process. The first optical observation was done by naked eye, followed by photographic meteor programs (e.g., *Ceplecha, 1957; McKinley, 1961*). Meanwhile, optical meteor observations were realized with the help of full automated camera systems and run quasi continuously on clear sky nights (e.g., *Weryk et al., 2013*).

A second possibility is the detection of meteors with radars. A radio signal is transmitted at a ground station and reflected by the plasma created by the ablating mete-

Chapter 1 Introduction

oroid. Depending on the geometry between the radar and the meteor echo and on the sensitivity of the system, different kind of meteor signals are observable (see section 2.2.2). The first meteor detections with radars were made around 1930 (*McKinley*, 1961). *Hey et al.* (1947) were the first, who used radar observations to determine the velocity of a specific meteor shower. Nowadays, radar systems benefit from the digitalization and run automatically 24 hours a day. Meteor trails were not only used for astronomical studies but also helped to gain information of the atmospheric background (e.g., *Hocking et al.*, 2001; *Stober et al.*, 2014; *Stober and Chau*, 2015; *Chau et al.*, 2017).

There are also measurement methods not related to the meteor plasma. Meteors are detectable by their infrasonic signature (e.g., *Silber et al.*, 2015). Furthermore, meteoroids can also be detected outside of the Earth's atmosphere by analyzing the impact craters on the surface of recovered satellites (*Love and Brownlee*, 1993), impact craters on the moon and the induced moon dust cloud (*Grün et al.*, 2011). In addition, satellites are able to observe the zodiacal dust cloud in our solar system (*Low et al.*, 1984; *Nesvorný et al.*, 2010).

This thesis focusses on radar observation of meteor head echoes. Therefore, the first quasi continuous meteor head echo observations with a high power large aperture radar are introduced and compared with an empirical meteor input function developed by *Fentzke and Janches* (2008). At a later time, the meteor head echo observations were extended by optical camera systems for the investigation of further physical parameters. In addition, a case study of a fireball detected as a head echo with an all sky meteor radar system is analyzed with respect to the trajectory, orbital elements and its ablation profile using a meteor ablation model.

The thesis is structured as follows: Chapter 2 gives a short overview of the current knowledge of the meteoroid ablation process, the sources of meteoroids and the different types of meteor radar echoes. The objectives of this thesis are stated in Chapter 3. Chapter 4 to 8 summarize the publications accompanied with this thesis, starting with the first observations of head echoes with the Middle Atmosphere ALOMAR Radar System (MAARSY) in Chapter 4. The observation of the Maribo fireball with an all sky meteor radar is described in Chapter 5. Chapter 6 shows the results of the first quasi-continuous meteor head echo observations, while Chapter 7 includes the comparison with an optical camera system located near the MAARSY radar. The last paper in Chapter 8 summarizes the study on meteor showers as observed with MAARSY. At the end an overall summary and outlook is given in the Chapter 9.

Chapter 2 General overview of the characteristics of meteors

2.1 Ablation of meteoroids

The ablation process of a meteoroid in the Earth's atmosphere is described by a set of differential equations including the equation of motion and the energy balance. In the following the underlying equations and assumptions are summarized and discussed with respect to the radar observations shown in this thesis.

The dynamic equation describes the deceleration of a meteoroid due to friction within the Earth's atmosphere (*McKinley*, 1961; *Stober et al.*, 2011b):

$$\frac{dv}{dt} = \frac{c_w A}{m^{\frac{1}{3}} \rho_m^{\frac{2}{3}}} \rho_{air} v^2 + \gamma \frac{M}{(R + z)^2} \quad (2.1)$$

with v the velocity of the meteoroid, t the time, ρ_m and ρ_{air} the density of the meteoroid and the surrounding atmosphere, m the meteoroid mass, $c_w = 1$ the drag coefficient and A a dimensionless shape factor. The second term on the right describes the acceleration due to the Earth gravity with γ the gravity constant, M and R the mass and the radius of the Earth and z the altitude of the meteoroid.

Radar systems only detect the plasma ball surrounding the meteoroid (head echo) or the plasma trail behind the meteoroid (specular or non-specular). In case of the head echo, it is assumed that the detected plasma moves with the speed of the meteoroid, enabling the possibility to get direct information on v and $\frac{dv}{dt}$. Some of the other parameters in equation 2.1 have to be assumed. The drag coefficient is often assumed to be unity because of the free flow regime (*Campbell-Brown and Koschny*, 2004). In addition it is assumed that the particle is a spherical body with a shape factor of $A = 1.21$ (*McKinley*, 1961). The density of the air in the mesosphere is often taken from atmospheric models as NRLMSISE-00 (*Picone et al.*, 2002). The gravitational term in equation 2.1 is only important for low speeds and low elevation meteors and often neglected in the mass determination or ablation models. Furthermore, the effect is too small to be resolved in radar velocity measurements.

The ablated mass due to thermal heating is described by the following equation (*Rogers et al.*, 2005):

$$\left(\frac{dm}{dt} \right)_{th} = -4A \left(\frac{m}{\rho_m} \right)^{2/3} P_v(T_m) \sqrt{\frac{\mu}{2\pi k_B T_m}} \quad (2.2)$$

Chapter 2 General overview of the characteristics of meteors

with P_v the saturated vapor pressure, T_m the temperature of the meteoroid, μ the mass of a meteoric atom and k_B the Boltzmann constant.

The vapor pressure can be calculated using the Clausius Clapeyron equation:

$$\log_{10}(P_v) = C_A - \frac{C_B}{T_m} \quad (2.3)$$

with the constants $C_A = 10.6$ and $C_B = 13500/16.120K$ for cometary or iron particles (*Öpik*, 1958; *Hill et al.*, 2005). An alternative for the calculation of the vapor pressures is the MAGMA model developed by *Fegley and Cameron* (1987). The MAGMA code enables the possibility to vary the chemical composition of the meteoroid and allowing for differential ablation (*Vondrak et al.*, 2008). The problem is that in most cases the chemical composition of the ablating meteoroid is not known. Therefore, assumptions for P_v and μ are necessary. Due to meteorite finds on the ground a chondritic composition is often used, including the main elements Oxygen, Iron, Magnesium, Silicon and Sodium.

The non-thermal mass loss of meteoroids due to collisions with atmospheric atoms is called sputtering (e.g., *Hill et al.*, 2005; *Vondrak et al.*, 2008; *Stober et al.*, 2011b):

$$\left(\frac{dm}{dt}\right)_{sp} = -2\mu A v \left(\frac{m}{\rho_m}\right)^{2/3} Y_{tot} \quad (2.4)$$

with the total sputtering yield Y_{tot} . The sputtering yield is a function of the properties of the atmospheric and meteoroid atoms (atomic numbers, atom masses and surface binding energy) and is in detailed described in *Tielens et al.* (1994) and *Rogers et al.* (2005). The number densities of the atmospheric constituents have to be taken from atmospheric models (e.g., NRLMSISE-00). Sputtering can be a main mass loss for very small meteoroids ($\sim < 10^{-10}kg$) with fast velocities (*Vondrak et al.*, 2008) and is the main explanation for high altitude detections (*Hill et al.*, 2004). When the meteoroid reaches the melting temperature, the thermal ablation dominates the mass loss by orders of magnitude.

The temperature of the meteoroid can be obtained with the heat balance equation, assuming an isotropic heat flux and isothermal heating (*Hill et al.*, 2005):

$$\frac{1}{2}\Lambda\rho_{air}v^3 = 4\epsilon k_B(T_m^4 - T_{air}^4) + \frac{Cm^{2/3}\rho_m^{2/3}}{A}\frac{dT}{dt} - \frac{L}{A}\left(\frac{\rho_m}{m}\right)^{2/3}\frac{dm}{dt} \quad (2.5)$$

with Λ the heat transfer coefficient, ϵ the emissivity, k_B the Boltzmann constant, T_{air} the air temperature, C the heat capacity of the medium and L the latent heat of fusion and vaporization. The terms are defined by the kinetic heating, radiative heating/cooling, heat capacity and vaporization. Again, in general the specific values for ϵ , C and L are material dependent and have to be assumed (chondritic).

Knowing the ablated meteoric atoms due to sputtering and thermal ablation, it is possible to calculate the released electron line density (*McKinley*, 1961):

$$q = -\frac{\beta}{\mu v} \frac{dm}{dt} \quad (2.6)$$

where β is the ionization efficiency, describing the ratio of produced electrons per released atoms. The ionization efficiency is an important parameter for the calculation

2.2 Sources of meteoroids

of the meteoroid mass, using the detected signal strength. β highly depends on velocity and composition, with a very strong gradient in the low velocity regime. *Jones (1997)* has done some theoretical and observational calculation on the ionization efficiency. Newer experimental values for β are given in *Thomas et al. (2016)* and *Moorhead et al. (2017)* using laboratory data and specular radar observations.

The light production of the meteor has a similar relation (*McKinley, 1961*):

$$I = -\frac{\tau}{2}v^2\frac{dm}{dt} \quad (2.7)$$

where τ is the luminous efficiency, describing the fraction of kinetic energy converted into light. τ depends on velocity, chemistry and the photometric pass-band (e.g., *Campbell-Brown et al., 2012*; *Weryk and Brown, 2013*).

Combining and solving these equations numerically makes it possible to simulate the complete ablation process in the Earth's atmosphere, which are called meteor ablation models (e.g., *Vondrak et al., 2008*; *Campbell-Brown, 2017*). There are some problems by using meteor ablation models to describe radar and optical observations. For example, the parameter space is large and the number of observable quantities is poor. Therefore, the lack of known values have to be filled with assumptions. Furthermore, the forward integration method in combination with a large computational time makes it not practical to fit the model on the observations. The last but maybe most complicated source of error, is the occurrence of fragmentation (e.g., *Babadzhanov, P. B., 2002*; *Cepilecha and Revelle, 2005*), increasing the parameter space by time of fragmentation, and the size and number of fragments. There is a meteor ablation model, solving the differential equations with a forward integrated 4th order Runge-Kutta method at the Leibniz-Institutde of Atmospheric Physics (IAP) (*Stober et al., 2011b*). Recently and motivated by the results presented here, the model includes a full-Earth geometry, solutions for differential/non-differential ablation and fragmentation.

2.2 Sources of meteoroids

The meteoroid population in our solar system is mainly divided into two components, called meteor showers and sporadic meteors. While a meteor shower is only visible for a limited time in the year, ranging from some hours to several weeks, sporadic meteor sources provide a continuous meteor flux into the Earth's atmosphere. Also the count rates, origins and mass distributions of shower and sporadic meteors differ significantly. Therefore, a separate treatment and analysis of both populations is necessary.

2.2.1 Meteor showers

Meteor showers consist of a number of meteors originating from the same radiant in the sky for a limited time in the year. They can be observed when the Earth crosses the orbit of a meteoroid stream. These meteoroid streams, in contrast to sporadic meteoroids, can sometimes be linked to a specific asteroid or comet with a similar orbit, called parent body. For example, the Geminid meteoroid stream, intersecting the Earth's orbit in December for over three weeks (e.g., *Brown et al., 2008*), can be directly linked to the asteroid 3200 Phaeton (*Whipple, 1983*). The dust particles

within the meteoroid streams are associated to be small dust fragments of the parent body released due to evaporation (comets), gravitational force or collisions. The link between a parent body to an observed meteor shower helps to understand the mass loss of asteroids and comets and provides an inside into the evolution of small meteoroids in our solar system (e.g., *Williams and Wu, 1993*; *Wiegert and Brown, 2005*). In addition, the radiant location of most of the known meteor showers are within the locations of the sporadic meteor regions. This fact gives evidence that the sporadic meteor background is the result of the dispersal of old meteor showers (*Brown et al., 2008*).

In the observational data meteor shower occur as an enhancement in the detection rate with a correlation in time, location and geocentric velocity (e.g., *Brown et al., 2008*; *Pokorný et al., 2017*). So far, 112 established meteor showers can be found in the shower list of the International Astronomical Union (IAU).

2.2.2 Sporadic meteors

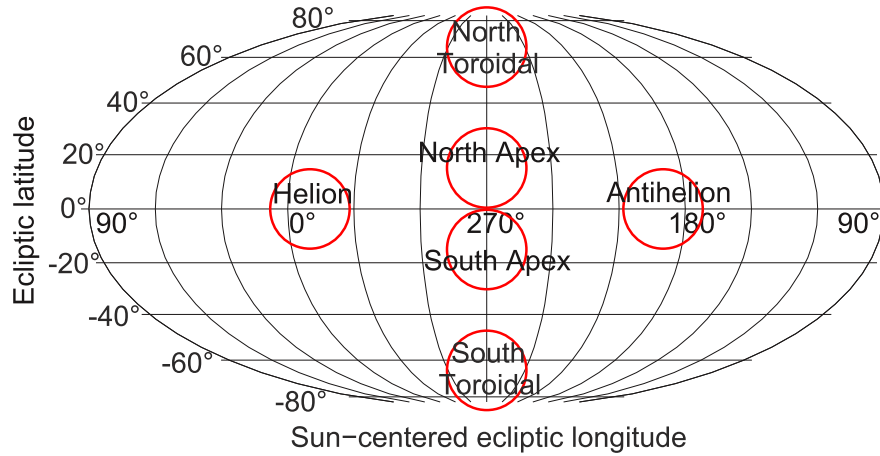


Figure 2.1 Location of the sporadic meteor sources in a sun-centered ecliptic coordinate system.

Meteors, which can not be assigned to a meteor shower, are called sporadic meteors (*Jones and Brown, 1993*). A clear separation between sporadic and shower meteors can be a difficult task since in most cases both populations overlap (*Brown et al., 2008*; *Pokorný et al., 2017*). By observing only a small number of sporadic meteors, the radiants seem to be randomly distributed. Nevertheless, the integration over a larger number of events yield the presence of six sporadic meteor sources, which were first completely classified in *Jones and Brown (1993)*. The location of the sporadic meteor sources are shown in Figure 2.1 in a sun-centered ecliptic coordinate system. In this coordinate system the rotation of the Earth is removed and the sun is located at the zero point. The sporadic sources are named after the location in the sky. The Helion (HE) source includes meteoroids coming from near the direction of the sun, while the Antihelion (AH) source is on the other side. Both sources are located on the ecliptic

plane (e.g., *McKinley*, 1961; *Jones and Brown*, 1993). The North/South Apex (NA, SA) mark meteors moving contrary to the Earth’s motion. These particles have the highest geocentric velocities, because the velocity of the Earth along its orbit around the sun add up with the meteoroid velocities (e.g., *Taylor*, 1997; *Chau and Woodman*, 2004). The North and South Toroidal sources (NT, ST) are the weakest consisting of meteoroids with high inclinations (e.g., *Fentzke and Janches*, 2008; *Campbell-Brown and Wiegert*, 2009). The different sporadic sources consist of dust released from different types of comets or asteroids (e.g., *Jones and Brown*, 1993; *Fentzke and Janches*, 2008). The Helion/ Antihelion complex is mainly composed of particles from Jupiter Familiar Comets (JFC) (e.g., *Nesvorný et al.*, 2010), which are comets with periods less than 20 years. The Apex and Toroidal sources are more associated to long period comets as Halley Type Comets (HTC) and Oort Cloud Comets (OCC) (e.g., *Nesvorný et al.*, 2011; *Pokorný et al.*, 2014). Also documented is a weak ring structure at about 55° around the Apex (*Campbell-Brown*, 2008). *Wiegert et al.* (2009) concluded by modeling the sporadic meteoroid complex that the ring structure can be explained with high-inclination dust, which evolves under the Poynting-Robertson drag and the Kozai effect.

2.3 Radar meteor echoes

Three different types of radar echoes exist related to the occurrence of ablating meteoroids in the atmosphere. Figure 2.2 shows examples of all types of radar meteor echoes observed with the HPLA radar MAARSY (see Figure 2.3 a). Figure 2.2 a) displays a typical meteor head echo as observed with HPLA radars. Due to the fact that these echoes are linked to the small plasma sphere surrounding the ablating meteoroid, HPLA radars are required to detect a considerable amount of events (e.g., Arecibo radar (*Janches et al.*, 2000), Jicamarca radar (*Chau and Woodman*, 2004), EISCAT radar (*Pellinen-Wannberg et al.*, 1998; *Kero et al.*, 2008), MU radar (*Kero et al.*, 2011)). The plasma sphere radii have sizes of a fraction of centimeters to a few meters depending on the mean free path length (altitude) and the meteoroid velocity (*Close et al.*, 2004). The small sizes of the targets correspond to low observable radar cross sections. Nevertheless, a small number of meteor head echoes are also observed with much smaller radar systems (e.g., *Janches et al.*, 2014; *Marshall et al.*, 2017).

Figure 2.2 b) shows a typical specular trail echo. These echoes are generally observed with smaller meteor radars (see Figure 2.3 b) and often used for atmospheric studies (e.g., *Stober et al.*, 2012). In the case of specular trail echoes the radar signal is scattered on the column of electrons (trail) created by the ablating meteoroid (e.g., *McKinley*, 1961). When the line of sight of the transmitted radio wave is perpendicular to the meteor trail, it reaches the specular condition and the radar cross section increases by orders of magnitudes. The detection condition is therefore more related to the geometry between the radar and the meteoroid entry angle. Due to the small observation volumes of HPLA radars, these specular echoes are more frequent in smaller radar systems, which very often have an antenna design to cover the whole sky. The downside of specular trail echoes, is that the meteor is only detected at the specular point. To get the whole trajectory information the combination of several radar systems is required

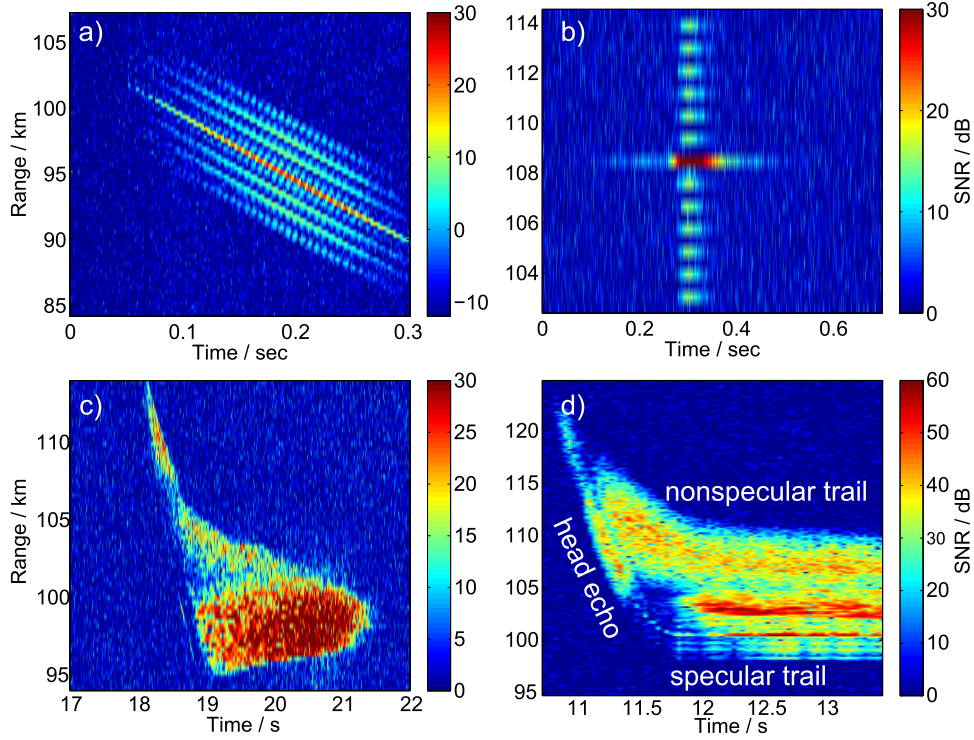


Figure 2.2 Different types of meteor radar echoes observed with MAARSY. a) Meteor head echo (from *Schult et al. (2017)*), b) specular meteor trail echo, c) non-specular trail echo, d) special meteor event producing all three types of radar echoes (from *Chau et al. (2014)*).

as it is done for the Canadian Meteor Orbit Radar (CMOR) (e.g., *Brown et al., 2004*).

The last type of meteor radar echoes is shown in Figure 2.2 c) and known as non-specular meteor trail. These echoes extend over several range gates and can last over several seconds and minutes (e.g., *Chau et al., 2014*). It is still an open question whether these long lasting trails are only the result of field aligned irregularities (e.g., *Dyrud et al., 2007; Close et al., 2008*) or if they are more linked to charged dust released from the meteoroid (*Kelley, 2004; Chau et al., 2014*). In some cases a corresponding head echo occurs some milliseconds before the non-specular trail evolves as shown in Figure 2.2 c) and d). In a rare number of events all three different types of radar echoes can be observed for a single meteoroid (see Figure 2.2 d).

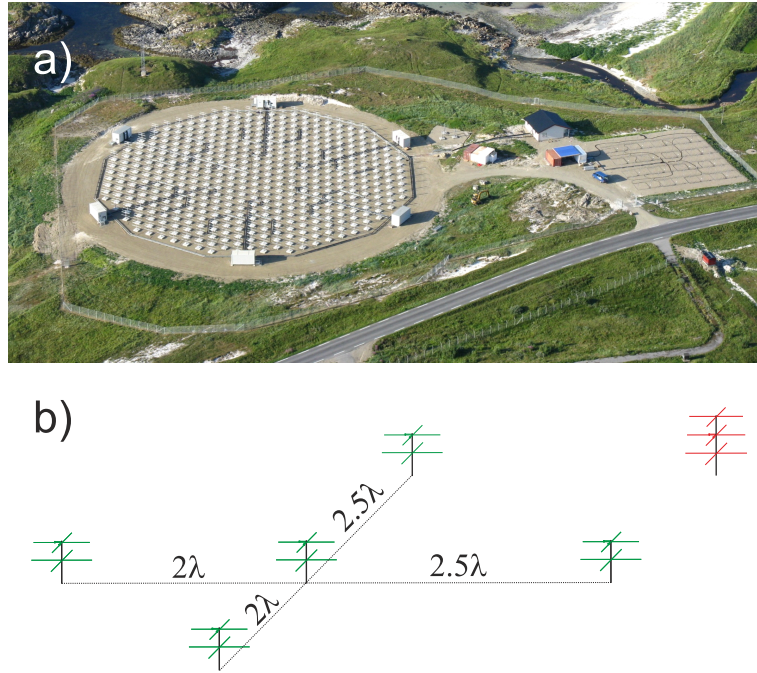


Figure 2.3 a): Photo of the MAARSY antenna array (courtesy of Ralph Latteck). Such HPLA radars are perfect for the detection of a large number of meteor head echoes. b): Sketch of a meteor radar for the detection of specular trail echoes. The red antenna transmits the radio signal, while the green antennas are for reception (with λ the wavelength of the transmitted signal).

Chapter 3 Objectives of the thesis

While continuous observation of specular meteor echoes are well established and exist for several years and on different locations (e.g., *Campbell-Brown*, 2008; *Stober et al.*, 2011a; *Janches et al.*, 2013), meteor head echo observations are rare and/or limited in observation time (e.g., *Close et al.*, 2002a; *Chau et al.*, 2007; *Kero et al.*, 2011; *Janches et al.*, 2014) and sometimes the radars lack of interferometric capabilities (e.g., *Janches et al.*, 2003; *Kero et al.*, 2008). The reason for this is that specular meteor radars are much smaller, cheaper and they are designed only for the detection of specular meteor trails (*Hocking et al.*, 2001). In contrast to that, HPLA radars are much more expensive, bigger and often build to investigate atmospheric or radio astronomical questions (e.g., EISCAT, Jicamarca, Arecibo). Since HPLA radars are often more sensitive (see table in *Pifko et al.* (2013)), these smaller particles of the meteoroid input are under-represented in the observations. In contrast to optical systems, radar systems have the advantage that they are independent on weather or light conditions. This thesis overcomes the lack of continuous meteor head echo observation by using a multi-target experiment mode developed and implemented for the HPLA - MAARSY. Therefore, a second data analysis pipeline for meteor head echo detections is developed, which does not interrupt the observation of other atmospheric phenomena as e.g., polar mesospheric or E-region echoes. The head echo analysis is fully automated, including event searching, cutting and trajectory/orbit/radar cross section analysis. The resulting large data set gives the possibility to investigate the sporadic meteoroid population. Furthermore, the large statistical amount of events helps to validate existing empirical models of the meteoroid input on Earth, so called meteor input functions (MIF). Also the meteor shower research, based on HPLA radars, was so far only realized in rare case studies (e.g., *Close et al.*, 2000; *Chau and Galindo*, 2008; *Kero et al.*, 2013) and can be expanded by a full year meteor shower survey with MAARSY. The observation of meteor showers with HPLA radars gives more insight into the particle size distribution within a meteoroid stream. Even less frequent than meteor head echo observations, are the simultaneous observation of head echoes with HPLA radars and optical systems. This limitation arises due to the fact that the short radar experiment time had to match with good weather conditions for the optical systems. Earlier radar- optical meteor head echo campaigns reported count rates ranging from 4 to 34 events (e.g., *Nishimura et al.*, 2001; *Campbell-Brown et al.*, 2012; *Michell et al.*, 2015). Continuous meteor head echo observation enlarge the time window for simultaneous observation. Combined measurements help to validate the measurement techniques, decrease the observational errors and add further independent meteor parameter, which are needed for detailed meteor ablation models.

Chapter 4 Meteor-head echo observations using MAARSY

Summary of :

Schult, C., G. Stober, J. L. Chau, and R. Latteck, Determination of meteor-head echo trajectories using the interferometric capabilities of MAARSY, *Ann. Geophys.*, 31, 1843-1851, 2013.

In the study of *Schult et al.* (2013) the first meteor-head echo observations with MAARSY are analyzed and a first statistical overview is given. The study is based on the measurements during the ECOMA rocket campaign in 2010. The measurement period lasted about two weeks between the 7th and 21th December, covering the maximum intensity of the Geminid meteor stream.

MAARSY (Middle Atmosphere Alomar radar system, location: 69.30°N, 16.04°E) is a phased array radar with a diameter of 90 and consists of 433 Yagi antennas (see Figure 2.3 a)). The complete antenna design and hard- and software details are described in *Latteck et al.* (2010). On reception, different sub-arrays can be defined, allowing the interferometric analysis of phase differences between the signals of the selected receiving channels. One sub-array can be defined as a Hexagon, consisting of 7 Yagi antennas or as an Anemone, consisting of 7 Hexagons. This technique helps to get information about the target location within the radar beam. Different experiment modes can be designed by changing the parameters in the pulse repetition frequency (PRF), wave form (mono pulse or various code forms), pulse length, sampling range, sampling resolution and number of coherent integrations.

During this early stage of the radar only eight receiving sub-arrays were available, including the whole antenna array and seven anemones for interferometry. In addition, the Yagi antennas had only one polarization plane and the long mono-pulse with a range resolution of 900 m was not ideal for the head echo observation.

The work describes how the raw data analysis is performed. The signal to noise ratio (SNR) of the raw voltage matrix was used for the identification of events and for the calculation of the radar cross section (RCS). For the determination of the meteoroid trajectory, the mean angle of arrival (MAOA) method was used. The cross correlation between the different receiving sub-arrays lead to the phase differences, which can than be converted with a least square fit into the angle of arrival of the signal. This is done

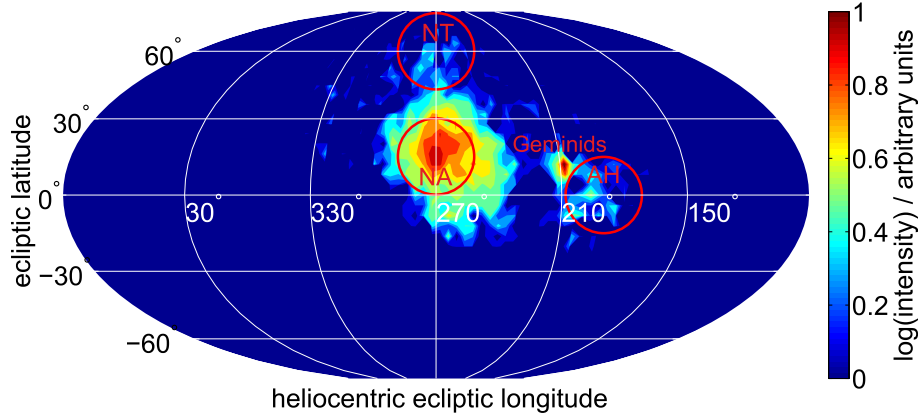
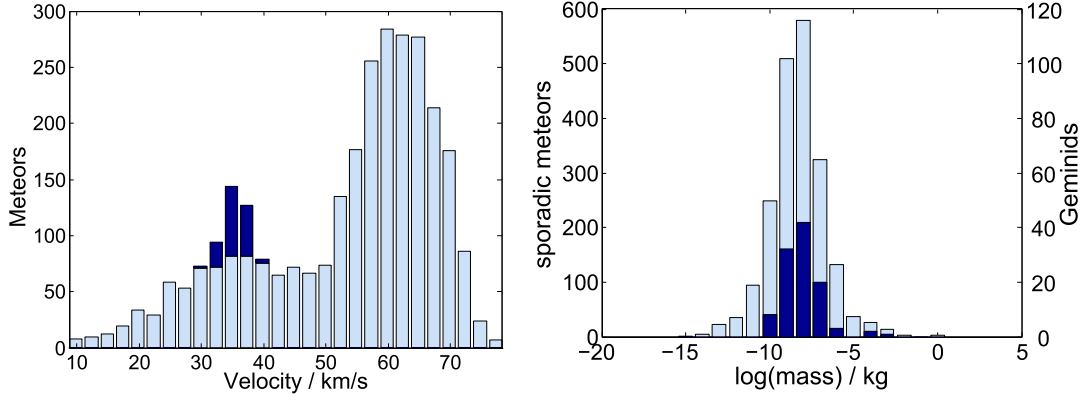


Figure 4.1 Meteor radiant density map of the MAARSY observations during the ECOMA rocket campaign in 2010. The observed sporadic sources and the location of the Geminid meteor stream are marked in red. Figure taken from *Schult et al.* (2013), Fig. 7.

for every received radar pulse, resulting, in combination with the range information, in a three dimensional trajectory. The velocity/deceleration curve is refined by calculating the phase differences of consecutive pulses of a single receiver. Knowing the location of the meteor within the radar beam, the RCS can be calculated by including the antenna gain and the background noise temperature.

During this measurement campaign about 2900 meteor head echoes were detected and analyzed. Most of them were associated to the North Apex sporadic source and a smaller fraction to the Antihelion and North Toroidal region. Only 5% had radiants and velocities corresponding to the Geminid meteor shower. The observed radiant density map in heliocentric ecliptic coordinates is shown in Figure 4.1. Due to the limited observation time and high latitudinal location of the radar system only a small fraction of the northern ecliptic sky is observed. The campaign based measurements show that MAARSY is a good tool to study the meteoroid background of the Earth.

Figure 4.2 a) and b) show the velocity and mass distribution as observed during the campaign. Light blue bars indicate sporadic meteors while the dark blue bars correspond to potential Geminid meteors. The fastest meteors in Figure 4.2 a) around 60 km/s belong to meteors from the North Apex direction, while the other sporadic sources add up to the second lower peak at 35 km/s. The Geminid shower is much lower in counts but adds a significant number of events to the 35 km/s peak. The velocity distribution looks similar to earlier head echo measurements with other HPLA radars at lower latitudes (*Chau and Woodman*, 2004; *Kero et al.*, 2011; *Close et al.*, 2007), but the ratio of the slower Antihelion and North Toroidal meteors is higher in the MAARSY observation. This can be explained with the location of the radar system (and time of observation) and the corresponding Earth filtering of low elevation meteors. Figure 4.2 b) shows that MAARSY is most sensitive to meteoroids with masses around 10 microgram ($10^{-8}kg$). Much higher masses are less likely to occur



(a) Figure taken from
Schult et al. (2013), Fig. 9.

(b) Figure taken from
Schult et al. (2013), Fig. 15.

Figure 4.2 Velocity and mass distribution observed during the ECOMA rocket campaign in 2010. Dark blue bars correspond to Geminid meteoroids.

within the small observation volume and for the detection of lower masses the system is not sensitive enough. It is important to note that the masses are calculated by using the dynamical equation, which includes the velocity and deceleration of the measurements and assumptions on the particle shape and density. For the Geminids a density of 2350 kg/m^3 was assumed while for the sporadics 1000 kg/m^3 seemed to be appropriate. Under these assumptions the mass distribution of the Geminid meteors has the same shape as the overall sporadic distribution.

Chapter 5 Radar observation of the Maribo fireball

Summary of :

Schult, C., G. Stober, D. Keuer, and W. Singer, Radar observations of the Maribo fireball over Juliusruh: revised trajectory and meteoroid mass estimation, MNRAS, 450, 1460-1464, 2015.

Schult et al. (2015) is a case study of the fireball event called Maribo above mid-Europe in January 2009. The name is based on a Danish city, where fragments of the fireball were found. For this special case optical and radar observation, as well as a chemical analysis were available. That made the Maribo fireball a perfect event for the utilization and testing of a meteoroid ablation model.

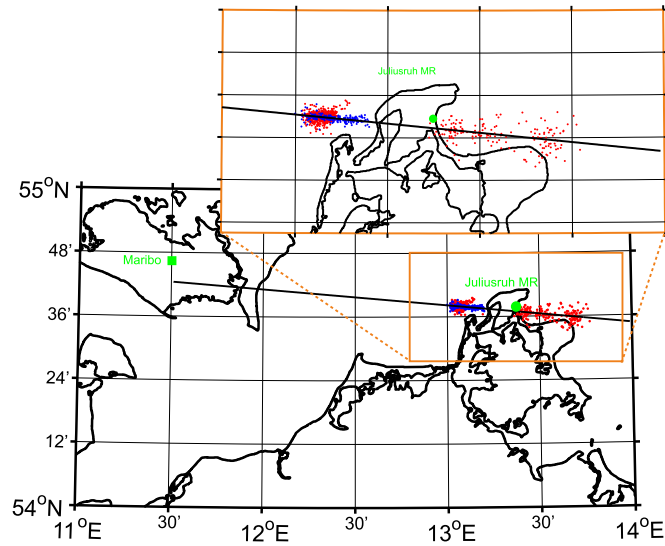


Figure 5.1 Maribo trajectory over Juliusruh as observed with a standard meteor radar. Blue dots correspond to head echo signals, while red dots belong to the non-specular echo. Figure taken from *Schult et al.* (2015), Fig. 2.

The meteor was observed with three different radar systems over Juliusruh. One system was a medium frequency (MF) radar, which only detected a very long lasting non-specular trail. The other two systems were a 53.5 and a 32.5 MHz specular radar system (see Fig. 2.3 b). The highest signal with the most information of the meteor trajectory was observed with the 32.5 MHz radar. The data analysis was done similar to *Schult et al.* (2013), considering the different receiving antenna arrays. Also important to note is that the raw data were not stored completely and a head echo was only observed in two consecutive ranges gates. To extend the length of the observed trajectory, parts of the non-specular trail were also used. Figure 5.1 shows the interferometric solution of the radar echo trajectory. The radar signals allow the reconstruction of the flight in the upper mesosphere, several kilometers before the optical detection started. The analysis shows that the fireball came from the east direction (Azimuth: 264.3°) with an elevation angle of 29.4° and a velocity of 28.5 km/s.

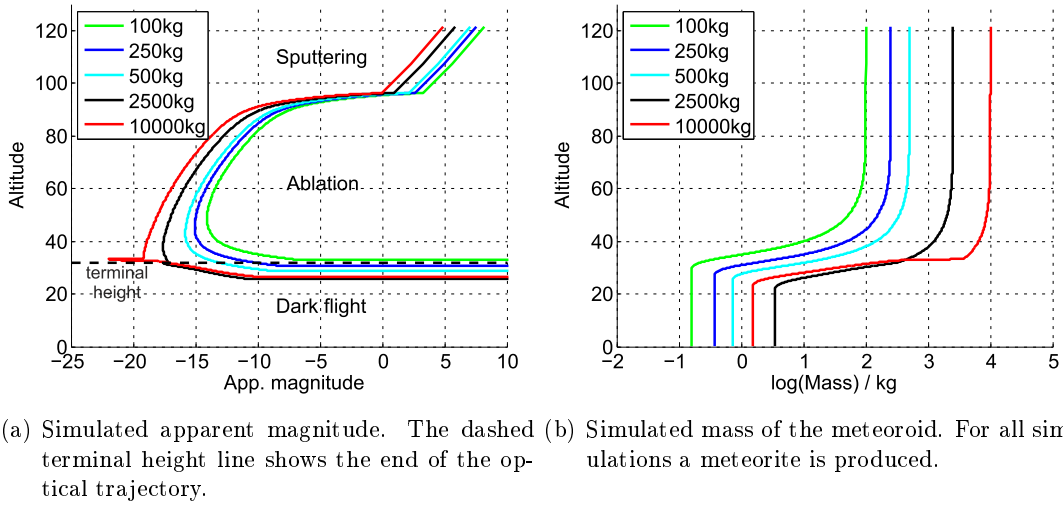


Figure 5.2 Ablation model of the Maribo fireball for five different initial masses. Figures taken from *Schult et al.* (2015), Fig. 5 and 6.

For the simulation of the ablation process of the meteoroid during the flight through the atmosphere a single-body meteor ablation model was used to get an estimation of the pre-entry meteoroid mass. The model is a forward integration model with a large computational time, making it impossible to fit the model directly on the measurements (*Stober et al.*, 2011b).

The model uses a fourth order Runge-Kutta method to solve the standard equations of motion for the deceleration and temperature from the energy budget and the ablation rate (e.g., *Öpik*, 1958; *Campbell-Brown and Koschny*, 2004). Also considered is the sputtering effect, what produces in some cases a sufficient ionization before the ablation starts. The vaporization pressure is calculated using the MAGMA equilibrium code (*Fegley and Cameron*, 1987; *Schaefer and Fegley*, 2004). For large objects a non-isothermal condition, with a fusion crust of a thickness less than 1 mm is assumed. In contrast to *Vondrak et al.* (2008), we assumed a constant chemical composition. For

Chapter 5 Radar observation of the Maribo fireball

the Maribo fireball, fragmentation was included with an uptake function.

As input parameters we used the information on the trajectory from the radar measurements and the chemical constituents from *Haack et al.* (2012). Then simulations were performed for five different initial masses ranging from 100 to 10000 kg. Figure 5.2 shows the results of the simulations for the apparent magnitude a) and the meteoroid mass b). Afterwards the model outcome was compared with the height of the first radar observation and the optical terminal height (horizontal dashed line in a)) to estimate, which initial mass fits best with the observation. Note, that for all initial masses a meteorite (ranging from 0.16 to 3.2 kg) is produced (b), which is an important fact since fragments were found on the ground. The final estimation resulted in a mass of about 250 kg but a precise estimation is quiet difficult.

For the case of the Maribo fireball the ablation model demonstrates that it is a good tool to combine all observations and to get an overview over the whole ablation process. The fact, that it is a forward integration model with a large parameter space (e.g., density, chemical composition, emissivity) and a long computational time, make it not feasible to be applied automatically to all meteor head echo observations.

Chapter 6 Quasi-continuous meteor head echo survey

Summary of :

Schult, C., G. Stober, D. Janches, and J. L. Chau, Results of the first continuous meteor head echo survey at polar latitudes, *Icarus*, 297, 1-13, 2017.

In *Schult et al.* (2017) the largest data set of meteor head echo measurements is presented. For the first time meteor head echoes were measured on a daily basis with a minimum of 50 % observation time per day for over two years. Since the measurements presented in *Schult et al.* (2013), MAARSY got several hard- and software updates. Some important upgrades are the second polarization plane and the extension to 16 receiving channels, allowing to increase the ambiguity area to 15.6° . In addition, a new experiment mode was designed to allow the detection of several mesospheric radar echoes such as polar mesospheric summer/winter echoes, E-region echoes and meteor head echoes. Due to the short duration of the head echoes and the fast transition between the different range gates, the head echo data were stored and analyzed separated from the original data set. In contrast to the measurements presented in *Schult et al.* (2013) the experiment is more sensitive, has a higher precision and is less vulnerable to interferometric ambiguity. For example, the pulse repetition frequency changed from 700 Hz to 1000 Hz and the range resolution decreased from 900 m to 300 m.

The new experiment mode started in November 2013 and is still in operation. For the study around 900000 meteors were analyzed with a mean detection rate of 2200 meteors per day. Figure 6.1 shows the location density of the detected meteors for 6 different times in the year (360° solar longitude correspond to 365 days). The white contour lines show which part of the sky was observed during the last 60° in solar longitude. The observation time (T) is weighted with the elevation angle (ele) of the region: $T = t_{mes} \cdot \sin(ele)^{1.5}$. This weighting was earlier reported by *Jenniskens* (1994) and *Kero et al.* (2013) and seems to fit perfect to our observations. From Figure 6.1 it can be seen that only a small region of the southern part of the celestial hemisphere is observed. While the North Toroidal source is visible during the whole year, a small part of the South Apex shows up for only about a quarter of the time. Due to the largest impact of Apex meteors, which is caused by their high velocities, and the seasonal effect, the count rates vary throughout the year from 1200 meteors per day, at the first

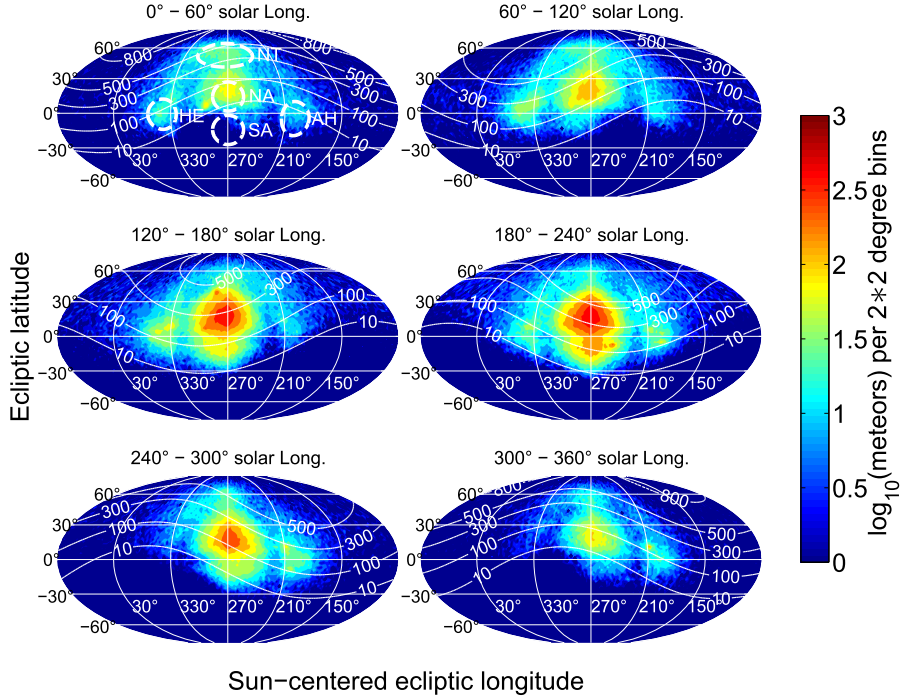


Figure 6.1 Density map of the detected meteor head echo radiants for 6 different solar longitudes. Each map shows the integrated detections over 60° solar longitude. The white contour lines show the weighted observation times for the different regions in space. The dashed ellipses in the first map mark the region of the observed sporadic sources. Figure taken from *Schult et al. (2017)*, Fig. 3.

half of the year, up to about 4000 meteors per day at the second half of the year. Also observed is a large change of the mean ablation heights (97.5 km to 102 km) and the mean elevation angles (20° to 40°).

The calculation of the masses is done similar to *Schult et al. (2013)* but due to the much larger data set (and the more precise measurements) a more detailed overview is given. Figure 6.2 shows a density plot of the observed mass distribution (x-axis) with the corresponding relative errors (y-axis). The error does not include assumptions on the particle density and shape or on the background density. The fact that the radar measures in principle only the radial component of the velocity makes the dynamical mass accuracy highly dependent on the elevation angle and the elevation error. Furthermore, heavy meteors experience only small deceleration in higher altitudes, requiring a precise measurement of the deceleration, what is not always achievable with the desired precision. Therefore all events with masses above 10 milligram have errors larger than 50% .

By comparing the dynamical masses of the different sporadic sources, it is shown that the Apex mean detected meteoroid mass is about $10^{-8.6}$ kg. The Helion/Antihelion sources peak at $10^{-7.7}$ kg, while the North Toroidal lies in between with $10^{-7.9}$ kg.

In the last section of *Schult et al. (2017)* the MAARSY observations were compared

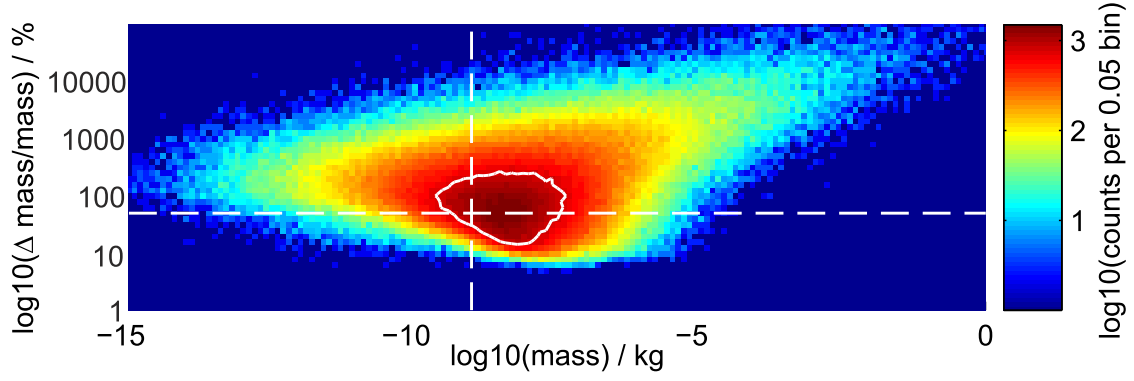
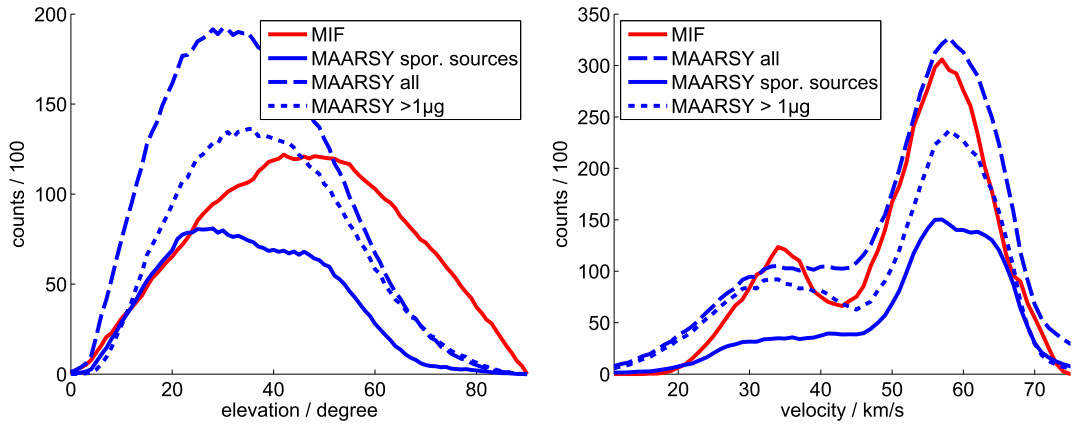


Figure 6.2 Density plot of the relative mass error vs. the dynamical mass. The horizontal dashed line marks 50% error and the vertical dashed line correspond to one microgram. The contour line represents the half maximum of the distribution. Figure taken from *Schult et al. (2017)*, Fig. 10.

with the meteor input function (MIF) developed by *Janches et al. (2006)*; *Fentzke and Janches (2008)* and *Fentzke et al. (2009)*. The MIF was a first attempt to explain the observations of different radar systems with a general meteor flux consisting of the six sporadic meteor sources. The comparison with other radar systems were done on short campaigns and often with the lack of interferometric capabilities. The MAARSY data set is therefore perfect for a comparison since it includes full trajectory information and covers the whole year cycle. A problem that still remains is the question of which part of the incoming flux is observed by the system. Three mainly empirical approaches were used to correct for elevation, velocity and mass selection effects. For the mass selection an one microgram cut off was chosen because the count rates decrease significantly below these mass threshold. Furthermore, for the velocity correction the Jones ionization β -formula (*Jones, 1997*) was used and the elevation dependence was corrected with the earlier mentioned $\propto \sin(ele)^{1.5}$ function. The results are shown in Figure 6.3 a) and b) for different MAARSY data sets. The blue lines represent the MAARSY observation for different filters (dotted: only meteors with dynamical masses above one microgram, dashed: all detections, solid: only events with radiants within the full width half maxima of the sporadic sources) and the red line shows the MIF prediction. The observations fit best by comparing only events with dynamical masses above one microgram. The MAARSY distribution including all detections slightly exceeds the predicted counts from the MIF. Assuming that the MIF predictions are correct, this confirms that a small fraction of the detected dynamical meteoroid masses are below one microgram. The discrepancies between the slope of the elevation and velocity distributions in Figure 6.3 can be ascribed to the differences in the locations of the meteor source regions between observation and MIF. While in the MAARSY observations only 41 % of the detections are within the full width half maxima of the six sporadic sources, the MIF assumes that all meteors originate from one of the six sporadic source regions. The MIF predicts a mean elevation angle of 40° over the whole year, while the mean

of the measurements is about 30° . The velocity distributions have the best agreement in the high velocity regime (45-70 km/s). Below 45 km/s the MIF underestimates the observed velocities except for the small peak around 35 km/s. This can be explained with the fact that in the MIF the Antihelion, Helion and North Toroidal sources have peak velocities of 35 km/s, while the MAARSY data show a peak velocity of 40 km/s for the North Toroidal source with a much broader width. The largest relative difference in the count rates occurs below ~ 25 km/s. Models for the Zodiacal dust cloud observation indicate that most of the particles should have velocities between 11 to 20 km/s (*Nesvorný et al.*, 2011; *Carrillo-Sanchez et al.*, 2015). In addition, radar observations have the lowest sensitivity to this part of the meteoroid influx due to the low ionization efficiency of slow meteors. In general it can be stated that the source regions of the MIF have to be adjusted and the number of slow meteors has to be increased to fit the MAARSY observation. Thus it is important to improve the concept of the radar filtering by using a radar cross section selection.



(a) Figure taken from *Schult et al.* (2017), Fig. 14. (b) Figure taken from *Schult et al.* (2017), Fig. 15.

Figure 6.3 Elevation and velocity distributions as observed with MAARSY and predicted by the meteor input function.

Chapter 7 Simultaneous radar and optical meteor measurements

Summary of :

Brown, P., G. Stober, C. Schult, Z. Krzeminski, W. Cooke and J.L. Chau, Simultaneous optical and meteor head echo measurements using the Middle Atmosphere Alomar Radar System (MAARSY): Data collection and preliminary analysis, *Planetary and Space Science*, 141, 25-34, 2017.

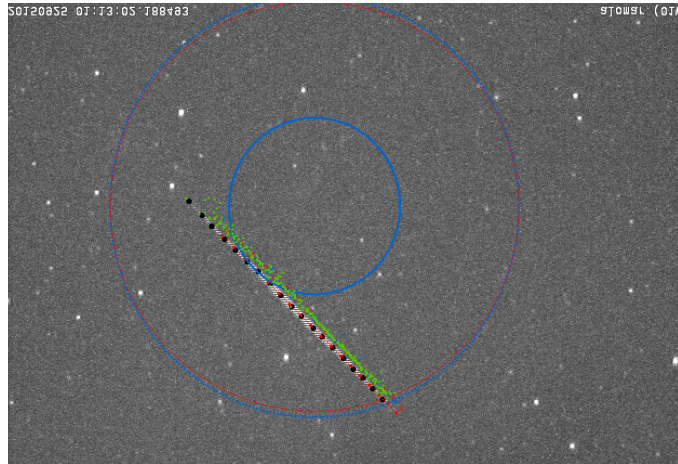


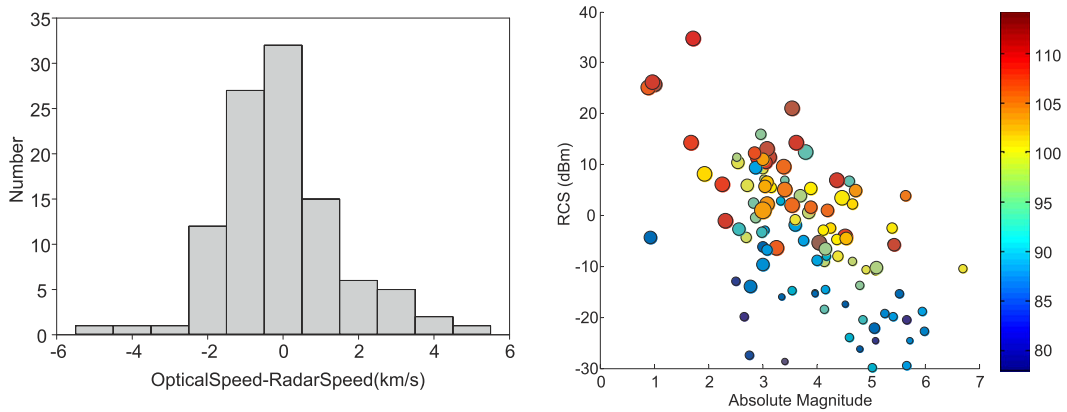
Figure 7.1 Meteor event observed simultaneously with a WATEC camera and as a head echo in the MAARSY data. Figure taken from *Brown et al.* (2017), Fig. 6 top, left.

In *Brown et al.* (2017) the initial results of simultaneous radar-optical meteor observations are shown. For that purpose the MAARSY head echo measurements (as shown in *Schult et al.* (2017)) were accompanied by camera systems located at the ALOMAR observatory and ~ 15 km south of MAARSY. At each site one wide field (Watec Ultimate H2, 768 \cdot 508 pixels, $14^\circ \cdot 11^\circ$ field of view) and one narrow field (AVT Prosilica GX1050, 1000 \cdot 1000 pixels, 6° diameter field of view) camera was installed,

Chapter 7 Simultaneous radar and optical meteor measurements

with limiting meteor magnitudes of about +5 and +7. The cameras were pointed to overlap in the altitude range of 100 km within the MAARSY main beam, where most of the MAARSY head echo detections occur. Figure 7.1 shows the trajectory of a simultaneous optical-radar event detected in September 2015. The picture displays the stacked meteor image from the WATEC ALOMAR camera with the interferometric solution (green dots) of the MAARSY detection. The blue circles indicate the 3dB line and the first minimum of the MAARSY radiation pattern. The figure shows that the optical and radar trajectories are parallel with a small positional offset. These small offsets seem to be random and are most likely caused by small phase errors between the MAARSY receiving channels.

The first analysis of 105 head echo- optical events shows a very good agreement in radiant and velocities with a median deviation of about 1.5° and 0.5km/s . For one third of the events the deviation in radiant is even less than one degree. The velocity difference between optical and radar observations is shown in the bar plot in Figure 7.2 a). This deviation correlates with the observed initial detection heights, which is in the case of MAARSY on average 1.3 km higher. Therefore, significant deceleration took place before the meteors are observed with the cameras. In most cases with earlier optical detection, the ablation started outside the main beam, where the sensitivity of MAARSY is orders of magnitude lower.



(a) Observed velocity difference between radar and optics. (b) Peak radar cross section vs. absolute magnitude at the same heights with color coded altitude in km.

Figure 7.2 Meteor event observed simultaneously with a WATEC camera and as a head echo in the MAARSY data. Figures adapted from *Brown et al. (2017)*, Fig. 7 and 9.

During times with suitable weather and daylight conditions, only about two percent of the MAARSY detections were observed by the narrow field camera systems. Using the limiting meteor magnitude of the narrow field camera and the magnitude-speed relation of *Verniani (1973)* leads to a mass threshold for MAARSY in the order of $10^{-9} - 10^{-10}$ kg for meteoroid velocities of 30 to 60 km/s.

Figure 7.2 (b) shows the peak radar cross section (RCS) versus the absolute mag-

nitude at the same height. The altitude is color coded and the dot size indicates the observed velocity (larger dots for higher velocities). As expected, it can be seen that brighter meteors correlate with larger radar cross sections. In addition, it is also shown that events with similar absolute magnitude have larger radar cross sections for higher velocities, which can be explained with the strong velocity dependence of the ionization efficiency. The scattering in Figure 7.2 b) is in the order of magnitudes (RCS variation for specific absolute magnitudes or vice versa) indicating the complex processes on ablation (chemistry, fragmentation, differential ablation) and the underlying meteor plasma scattering. A detailed interpretation of this data requires the simulation of the plasma scattering similar to *Marshall and Close* (2015) but for the MAARSY frequency of 53.5 MHz in addition with ablation modeling.

For a significant amount of events, the RCS curves show large oscillations and jumps, while the light curves show a smooth behavior. It is an open question if this behavior is caused by fragmentation, resulting in multiple target scattering, or by the differential ablation of various species, which do not show up in the optical data.

Chapter 8 Meteor head echo shower survey with MAARSY

Summary of :

Schult, C., P. Brown, P. Pokorný, G. Stober and J. L. Chau, A meteoroid stream survey using meteor head echo observations from the Middle Atmosphere ALOMAR Radar System (MAARSY), 2018, submitted manuscript, Icarus

Schult et al. 2018 is a study on meteor showers detected within the MAARSY meteor head echo data set. In contrast to previous meteor head echo shower observations, where dedicated measurements were conducted for specific and established meteor showers, the continuous observation with MAARSY offers the possibility to run an independent meteor shower search. Therefore, a 3D wavelet algorithm, which was so far used for specular meteor data (*Galligan, 2000; Brown et al., 2008; Pokorný et al., 2017*), is used to search for local maxima in the ecliptic longitude, latitude and geocentric velocity space. This is done for every bin in solar longitude. In a second step, the identified maxima are linked to get an idea of the apparent motion and duration of the potential showers. This procedure results in a list of potential showers (the list can be found in the supplementary material of (*Schult et al., 2018*)), which was afterwards checked manually. The manual check is necessary because in some cases showers are not linked successfully due to a low number of meteor detections of the shower or a large scattering in the radiant position. At the end, 33 showers were identified in the data set. The list of all identified showers is shown in Table 8.1. Listed is the shower name (IAU code), the corresponding shower numbers (No.), start, maximum and end time in solar longitude ($\lambda_s, \lambda_m, \lambda_e$), the duration, the radiants (α_g, δ_g), radiant drift ($\Delta\alpha_g, \Delta\delta_g$), radiant errors ($\pm\Delta\alpha, \pm\Delta\delta$), wavelet coefficient at the maximum ($W_{c_{max}}$), sigma above the background (σ_{wave}) and the geocentric velocity (V_g). Information and plots of the linked shower numbers can be found in the supplementary material of *Schult et al. (2018)*. The location of the showers in sun-centered ecliptic coordinates is shown in Figure 8.1.

In contrast to the shower surveys of specular meteor radar, the number of detected showers is lower. *Brown et al. (2010)* reported the detection of 117 meteor showers with the CMOR system, while *Pokorný et al. (2017)* found 58 shower in the data of the southern Argentina radar SAAMER. The discrepancies can partly be explained by

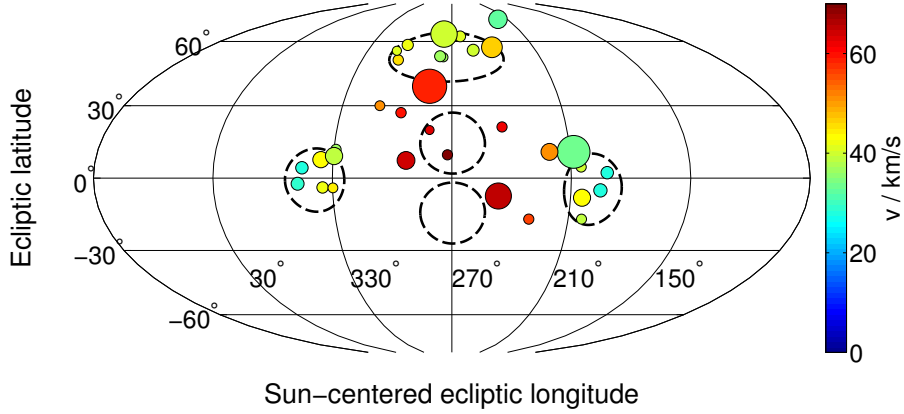


Figure 8.1 Radiant positions of all showers observed with MAARSY. The geocentric velocity is color coded and the marker size represents the strength of the shower above the background. The location of the sporadic meteor sources are marked with dashed ellipses.

the differences in the statistical quantity of the data sets (one million meteors in the SAAMER data, three million with the CMOR system). Another important aspect is the geographical latitude of the MAARSY radar. Only the northern part of the celestial sky is observed with the radar system during the whole year, while the southern part below $\sim -30^\circ$ is completely missing (see Figure 3 in *Schult et al. (2017)*). On the other side there is also a physical reason for the lower number of meteor showers in the head echo survey compared to the specular radars. Meteor streams are supposed to be richer in larger particle (*Jenniskens, 2006*) since smaller particles are more efficiently removed from the stream due to radiation pressure (*Burns et al., 1979*). The higher sensitivity of the MAARSY radar (10^{-9} to 10^{-10} kg (*Schult et al., 2017; Brown et al., 2017*) in contrast to 10^{-7} kg at 30 km/s for CMOR) leads to the detection of smaller particles, which might already passed to the sporadic background.

Although meteor showers below a geocentric velocity of 27 km/s exist, none of these showers are visible in the MAARSY data set. Due to the strong decrease in the ionization efficiency at slow velocities, only larger meteoroids can produce a sufficient ionization to be detected by the radar system. Furthermore, the small observation volume of the system makes it less likely to detect a sufficient amount of these larger objects. In contrast to that, MAARSY seems to be a good tool for the observation of faster meteor showers. This is also the case for the sporadic meteors, where the fast Apex sources dominate the observations (e.g., *Janches et al., 2006; Chau et al., 2007*), while for specular systems the Helion/Antihelion complex has a stronger relative signal (e.g., *Campbell-Brown and Jones, 2006*). Specular radar systems show a reduced detectability for faster meteors, which typically ablate at higher altitudes, due to the initial trail radius effect.

Figure 8.2 shows the comparison of the observed shower durations between the MAARSY and the CMOR systems in solar longitudes. In some cases the differences are very large and reach up to several weeks. The largest discrepancies are observed for

low velocity showers. Again, this observation underlines the aspect that the systems observe different parts of the particles within the meteoroid stream.

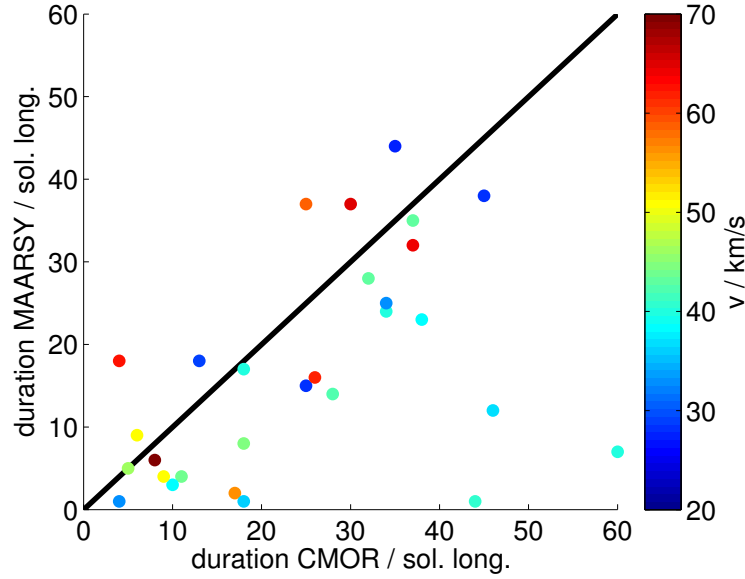


Figure 8.2 Comparison of the meteor shower duration as observed with MAARSY and the specular meteor radar system CMOR.

To get an estimation of the masses of the detected stream meteoroids, the dynamical masses are calculated using the equations in *Schult et al.* (2013, 2017). All events within 3° of the calculated wavelet radiant position (corrected for radiant drift) and 3 km/s in speed are assumed to be shower meteors of the same stream. Furthermore, only meteors with uncertainties in the dynamical masses of less than 50% are used (compare Figure 10 in *Schult et al.* (2017)).

The selected meteors are used to calculate the mass indices of the four strongest meteor showers in the data set. The mass index s is the exponent of the assumed power law $dN = Cm^{-s}dm$ with dN , the number of meteoroids with masses between m and $m + dm$ and C a normalization constant (*Cepke et al.*, 1998). The index s indicates if the majority of the mass of a population of meteoroids is concentrated in larger or in smaller particles. Smaller values of s indicate that more mass is accumulated in larger particles ($s = 2$ represents an equally distribution of mass). The cumulative mass index is fitted using the Multi-Nest algorithm described in *Pokorný, P. and Brown, P. G.* (2016). For a comparison with the shower mass indices, the mass indices for the sporadic background (all meteors) and for specific velocity regimes (33-38, 40-45 and 63-68 km/s) of the sporadic backgrounds are also examined. For the total data set of the sporadic background a value for s of -2.07 is obtained, which is similar to the values of the model of *Grün et al.* (1985). The values for sporadic velocity bin data are smaller: -1.701 (33-38 km/s), -1.686 (40-45 km/s) and -1.988 (63-68 km/s). These values are slightly lower than the values of the showers with similar speeds: Orionids ($s = -1.95$), Geminids ($s = -1.64$), Quadrantids ($s = -1.56$) and Perseids ($s = -1.45$). At larger

sizes the values for shower indices are typically higher ($s > 1.6$, *Blaauw et al.* (2011)). The Orionids are the exception with a very high mass index of -1.95. *Kero et al.* (2011) observed a similar mass index for the Orionids of about 2 using the radar cross section of the shower meteors. The Orionids, as a Halleyid meteor shower, seem to be richer in smaller particles.

Table 8.1 Meteor showers identified in the MAARSY head echo survey. The table shows shower number from the wavelet analysis (No.), solar longitude of first/end detection (λ_s and λ_e), solar longitude of the wavelet maximum λ_m , duration, geocentric right ascension/declination (α_g/δ_g), radiant drift and errors ($\Delta\alpha_g/\pm(\Delta\alpha)/\Delta\delta/\pm(\Delta\delta)$), wavelet coefficient at the maximum (W_{cmax}), geocentric velocity (V_g).

IAU code	No.	λ_s	λ_m	λ_e	duration	α_g	δ_g	$\Delta\alpha_g$	$\pm(\Delta\alpha)$	$\Delta\delta_g$	$\pm(\Delta\delta)$	W_{cmax}	σ_{wave}	V_g
BTA	1 90 92 88	85.5	98.5	102.5	18	85.7	21.1	0	0	0	0	71.3	15.7	29.2
PPS	2 5	99.5	111.5	116.5	18	23.1	30.9	0.75	0.07	0.61	0.08	160.6	7.6	62.7
TPR	4 6	105.5	108.5	113.5	9	45.9	48.7	0	0	0	0	33.2	9.3	50.8
PER	7 8 9	112.5	140.5	148.5	37	48.6	58.2	1.32	0.03	0.32	0.01	1140.2	109.1	58.7
ZCY	10 11 24	10.5	14.5	18.5	9	300.4	39.7	0	0	0	0	76.4	11.9	42.5
ZCA	13 16 17	151.5	163.5	164.5	14	139.7	11.7	0	0	0	0	43.1	12.2	42.5
KLE	15 18 19 21 29	162.5	181.5	196.5	35	162.2	15.7	0.77	0.04	-0.3	0.03	104	24.7	42.9
DPL	22	174.5	176.5	177.5	4	147.2	9	0	0	0	0	30.3	9.1	43.8
STA-TA	23 26 36 37	181.5	195.5	218.5	38	30.4	7	0.77	0.03	0.3	0.02	82.8	16.7	28.1
ORI	25 28	189.5	210.5	225.5	37	97.2	16	0.85	0.01	0.03	0.01	430.5	64	64.6
LMI	27 31 35	192.5	210.5	215.5	24	161.4	37.2	1.16	0.09	-0.66	0.06	79.1	10.2	59.3
CTA-ETT	32 34 40	203.5	222.5	226.5	24	64.8	26	0.74	0.34	0.14	0.14	38.8	9.8	40.2
NTA-TA	39 41	217.5	227.5	231.5	15	56.7	22.2	0.93	0.07	0.05	0.05	79	14.7	27.9
NOO	42 45	231.5	244.5	258.5	28	88.7	15.4	0.67	0.02	-0.06	0.02	103.7	27.3	42.7
LEO	43	233.5	236.5	238.5	6	154.4	20.8	0.88	0.09	-0.52	0.21	105.9	9.7	69.3
GEM	46	246.5	261.5	270.5	25	113.1	32.6	1.19	0.03	-0.17	0.03	1018.2	101	33.1
MON	48	255.5	257.5	257.5	3	100.2	6.3	0	0	0	0	29.4	9.6	38.6
HYD	49	256.5	257.5	257.5	2	125.9	2.1	0	0	0	0	27	9.8	56.7
DAD-NID	50	256.5	256.5	256.5	1	205.8	61.5	0	0	0	0	67.7	11.2	40.8
DLM	51	264.5	268.5	279.5	16	162.7	30.1	0.9	0.06	-0.39	0.03	78.5	9.8	61.7
URS	53	270.5	270.5	270.5	1	221.9	75	0	0	0	0	123.6	32.3	32.6
JLE	54	281.5	281.5	284.5	4	148	24.4	0	0	0	0	89.3	27.1	50.6
QVA	55 56	281.5	283.5	287.5	7	230.3	49.9	0.6	0.13	0.16	0.08	659.3	65.1	40
LBO	58 62	284.5	292.5	300.5	17	214.9	46.7	0.76	0.13	-0.33	0.09	79.9	13.6	40
XCB	59	291.5	293.5	298.5	8	248.2	29.6	0.48	0.09	-0.04	0.09	59	10.1	44.9
Part of CB	60 61	293.5	295.5	301.5	9	229	36.6	0.8	0.2	-0.22	0.21	53.2	8	36.4
TCB	63	298.5	298.5	298.5	1	232.9	35.7	0	0	0	0	82	11.5	36.4
Part of ARC	64 65	30.5	31.5	34.5	5	317.1	42.8	0	0	0	0	45.3	8	41.4
LYR	66	31.5	32.5	35.5	5	272	33.6	0.53	0.17	-0.38	0.06	208.1	40.2	46.2
ETA	67 70	34.5	45.5	65.5	32	337.5	-1.6	0.7	0.01	0.35	0.01	346.9	29.8	64.3
NOC	68 69 71	44.5	47.5	55.5	12	10.4	17.3	0	0	0	0	40.5	9.8	36.6
ZPE	72 73 74 75 82 83 85 86 91	53.5	86.5	96.5	44	69.8	26.4	0	0	0	0	83.8	14.4	27.7
ARI	76 77 78 79 80 81 84 87 89	66.5	82.5	88.5	23	47.1	27	0.37	0.13	0.45	0.1	193.3	27.9	38.6

Chapter 9 Summary and outlook

The observation of meteor head echoes requires HPLA radars, which are very large and expensive. These HPLA systems are often build to meet various scientific goals like atmospheric phenomena or astronomical sources. Therefore, dedicated and continuous experiments are rare and often done on a campaign basis for the duration of several hours or days. In this thesis the first and so far unique quasi continuous meteor head echo observations with the HPLA radar MAARSY for a period of more than two years are presented.

In *Schult et al. (2013)* a campaign based meteor head echo experiment during the time of the Geminids, within an early stage of the MAARSY radar, was presented. The observation showed that MAARSY is sensitive enough to detect a sufficient amount (~ 2900) of meteor head echoes. Due to the interferometric capabilities of the radar, three sporadic sources and the Geminid meteor shower could be identified in the data set.

The limited receiver constellation during this early measurements and the specific head echo experiment mode was still a limiting factor for meteor studies. To overcome the issue of the limiting observation time, an experiment mode was implemented, allowing the observation of several different mesospheric echoes at the same time. Out of these data set the meteor head echoes were extracted and a full year meteor climatology was presented in *Schult et al. (2017)*. The high northern latitude of the radar results in a strong seasonal behavior of the meteor count rate, varying from 1200 events in the first half of the year to up to 4000 in the second half. Then the Apex sporadic meteor source dominates the observations. The seasonal effect is also visible in the ablation heights (varying from 97.5 to 102 km) and in the corresponding elevation angles (20° to 30°).

A mass estimation for the detected meteoroids was done by using a dynamical approach that involves the measured quantities of speed, deceleration and altitude in combination with assumptions on particle density, particle shape and atmospheric density. These mass calculation gives a good overview of the observed masses in a statistical sense, but generally suffers from large errors, especially for low elevation angles or high mass events. Due to the different mean velocities of the sporadic sources, MAARSY detects the lowest meteoroid masses in the Apex direction ($10^{-8.6}$ kg). The mean masses of the Helion/Antihelion complex is nearly one order of magnitude larger ($10^{-7.7}$ kg). The North Toroidal meteoroid masses are in between ($10^{-7.9}$ kg).

A comparison of the radar measurements with the meteoroid input function developed by *Fentzke and Janches (2008)* showed a good agreement in the overall count rates by filtering masses below one microgram. The measurements showed that a significant part of the observed meteors are coming from outside of the sporadic source

Chapter 9 Summary and outlook

regions (only 40% are within the full width half maxima of the defined sources). These events are so far not included in the MIF. Furthermore, the locations and widths of the sporadic sources in the MIF need to be adjusted to reproduce the MAARSY observations. It is shown, that for high latitude meteor observations the low elevation meteors have the main contribution to the meteoroid influx. These low elevation meteors were neglected in a previous study of *Pifko et al.* (2013) to fit the prediction of the MIF to the MU radar observations. This assumption does not hold in the case of MAARSY. Another important aspect is the fast decrease in the predicted count rates for the slowest meteors. In this velocity regime the MIF underestimates the observed meteoroid flux.

The quasi continuous head echo observations made it possible to realize the first meteor head echo shower survey. In the past meteor showers were observed with optical or specular radar systems. Meteor head echo observations were only done for specific known showers and not during the whole shower period. Due to the fact that HPLA radars are more sensitive than specular meteor radars, smaller particles within the meteoroid stream can be observed. The detection of the smallest particles within a meteoroid stream is of great interest, since smaller particles should be removed efficiently from the stream due to the radiation pressure of the sun (*Burns et al.*, 1979). The first meteor head echo survey is presented in *Schult et al.* (2018), where it is shown that the duration and intensity differ a lot between head echo and specular observations. 33 meteor showers were found in the MAARSY data set and only about 1% of the overall detections could be associated with shower meteors. In comparison to that *Brown et al.* (2008, 2010) had found 109 meteor showers within the CMOR observations and about 10% of the detection were associated with shower meteors. Nevertheless, it is shown that HPLA radar observations are able to detect a large number of meteor showers with particles masses even below 10^{-9} kg for the faster showers. The mass indices for the four most significant showers were calculated. The indices range from 1.5 to 1.6 for the Geminids, Quadrantids and Perseids, while for the Orionids a mass index of about 2 was observed. The Orionids, as a Halley-type meteoroid stream, seems to consist of a significant number of smaller particles. Future specific single shower analysis might offer the possibility to study the orbital evolution and separation of the particles within the meteoroid stream since the specular and head echo systems observe different particle sizes.

The most important and necessary future work will be the improvement of the meteoroid mass determination in addition with the estimation of further parameters like particle density, fragmentation and composition. To address this topic several ideas and plans are in preparation and already partly realized. An alternative mass estimation can be done by using the measured radar cross section of the meteor (*Close et al.*, 2004; *Marshall and Close*, 2015). Unfortunately, at least dual frequency measurements are needed to get an idea of the plasma density around the ablating meteoroid. In winter 2016/17 dual frequency measurements with the EISCAT and MAARSY radars were conducted. For this experiment the EISCAT system (929 MHz, located near Tromsø) pointed in the observation volume of the standard MAARSY experiment. Hundreds of common meteor head echoes were detected and a precise analysis with a finite difference time domain (FDTD) backscatter model is planned. These observation might help to refine the estimated dynamical masses or it might lead to an empirical function

for the MAARSY single frequency observations. In addition, combined optical observations were also realized and a first overview is shown in *Brown et al. (2017)*. There it is shown that the observations fit quite well by comparing the trajectory parameters. The relation between the optical count rates and the detection by the radar system suggests a limiting mass for MAARSY in the order from 10^{-9} to 10^{-10} kg for velocities from 30 to 60 km/s. This estimation yields slightly lower masses than what was used for the comparison with the meteoroid input function. The comparison of the optical magnitude and the radar cross section of simultaneous events show brighter events for larger RCS as it is predicted by scattering theory, but the point scattering is very high and reaches up to tenth of dB. Also shown in the paper is that for a significant number of events the RCS curves seem to oscillate, while the light curve has a smooth behavior. The scattering as well as the differences in the light/RCS curves might be a consequence of fragmentation or differential ablation. To get an idea of the physical processes, producing the strange ablation curves, detailed analysis in combination with ablation modeling is needed.

In *Schult et al. (2015)* a single body ablation model was used for the bright meteor event "Maribo". The fireball was observed with a standard meteor radar, a video camera and by naked eyes. In addition some meteorite fragments were found, which gave an idea of the chemical composition. In combination with the trajectory information of the radar observation, the ablation process was simulated for different masses. The model results yield to an estimation of the initial meteoroid mass of at least 250 kg, which is three times larger than the previous estimation based on an isotope analysis of the found fragments. The large parameter space and the fact, that the ablation simulation is a computational time intensive forward model, makes the implementation for the millions of head echoes of the MAARSY standard experiment inefficient. In a first step a refinement of the ablation model by using the combined radar-optical measurements is planned. Furthermore, the combined observation help to reduce the parameter space of the model. With an estimation of observed parameters, it is possible to create a look-up-table for a variety of different meteors, allowing a faster classifying of the ablation curves.

Bibliography

- Babadzhanov, P. B., Fragmentation and densities of meteoroids, *A&A*, *384*(1), 317–321, doi:10.1051/0004-6361:20020010, 2002.
- Blaauw, R. C., M. D. Campbell-Brown, and R. J. Weryk, A meteoroid stream survey using the canadian meteor orbit radar - III. mass distribution indices of six major meteor showers, *Monthly Notices of the Royal Astronomical Society*, *414*(4), 3322–3329, doi:10.1111/j.1365-2966.2011.18633.x, 2011.
- Brown, P., J. Jones, R. J. Weryk, and M. D. Campbell-Brown, The velocity distribution of meteoroids at the earth as measured by the canadian meteor orbit radar (CMOR), *Earth, Moon, and Planets*, *95*(1), 617–626, doi:10.1007/s11038-005-5041-1, 2004.
- Brown, P., R. Weryk, D. Wong, and J. Jones, A meteoroid stream survey using the canadian meteor orbit radar: I. methodology and radiant catalogue, *Icarus*, *195*(1), 317 – 339, doi:http://dx.doi.org/10.1016/j.icarus.2007.12.002, 2008.
- Brown, P., D. Wong, R. Weryk, and P. Wiegert, A meteoroid stream survey using the canadian meteor orbit radar II: Identification of minor showers using a 3D wavelet transform, *Icarus*, *207*, 66–81, 2010.
- Brown, P., G. Stober, C. Schult, Z. Krzeminski, W. Cooke, and J. Chau, Simultaneous optical and meteor head echo measurements using the middle atmosphere alomar radar system (MAARSY): Data collection and preliminary analysis, *PSS*, *submitted*, –, 2017.
- Burns, J. A., P. L. Lamy, and S. Soter, Radiation forces on small particles in the solar system, *Icarus*, *40*(1), 1 – 48, doi:https://doi.org/10.1016/0019-1035(79)90050-2, 1979.
- Campbell-Brown, M., High resolution radiant distribution and orbits of sporadic radar meteoroids, *Icarus*, *196*(1), 144 – 163, doi:https://doi.org/10.1016/j.icarus.2008.02.022, 2008.
- Campbell-Brown, M., Modelling a short-wake meteor as a single or fragmenting body, *Planetary and Space Science*, *143*(Supplement C), 34 – 39, doi:https://doi.org/10.1016/j.pss.2017.02.012, sI:Meteoroids 2016, 2017.
- Campbell-Brown, M., and P. Wiegert, Seasonal variations in the north toroidal sporadic meteor source, *Meteoritics & Planetary Science*, *44*, 1837–1848, 2009.

- Campbell-Brown, M. D., and J. Jones, Annual variation of sporadic radar meteor rates, *Mon. Not. R. Astron. Soc.*, *367*, 709–716, 2006.
- Campbell-Brown, M. D., and D. Koschny, Model of the ablation of faint meteors, *A & A*, *418*, 751–758, 2004.
- Campbell-Brown, M. D., J. Kero, C. Szasz, A. Pellinen-Wannberg, and R. J. Weryk, Photometric and ionization masses of meteors with simultaneous EISCAT UHF radar and intensified video observations, *Journal of Geophysical Research: Space Physics*, *117*(A9), n/a–n/a, doi:10.1029/2012JA017800, a09323, 2012.
- Carrillo-Sanchez, J. D., J. M. C. Plane, W. Feng, D. Nesvorny, and D. Janches, On the size and velocity distribution of cosmic dust particles entering the atmosphere, *Geophys. Res.*, *42*, 6518–6525, doi:10.1002/2015GL065149., 2015.
- Ceplecha, Z., Photographic geminids 1955, *Bulletin of the astronomical institutes Czechoslovakia*, *8*, 51–61, 1957.
- Ceplecha, Z., and D. O. Revelle, Fragmentation model of meteoroid motion, mass loss, and radiation in the atmosphere, *Meteoritics & Planetary Science*, *40*(1), 35–54, doi:10.1111/j.1945-5100.2005.tb00363.x, 2005.
- Ceplecha, Z., J. Borovicka, W. G. Elford, D. O. Revelle, R. L. Hawkes, V. Porubcan, and M. Simek, Meteor phenomena and bodies, *Space Science Reviews*, *84*, 327–471, 1998.
- Chau, J. L., and F. Galindo, First definitive observations of meteor shower particles using a high-power large-aperture radar, *Icarus*, *194*(1), 23 – 29, doi:http://dx.doi.org/10.1016/j.icarus.2007.09.021, 2008.
- Chau, J. L., and R. F. Woodman, Observations of meteor-head echoes using the Jicamarca 50 MHz radar in interferometer mode, *Atmos. Chem. Phys.*, *4*, 511–521, 2004.
- Chau, J. L., R. F. Woodman, and F. Galindo, Sporadic meteor sources as observed by the Jicamarca high-power large-aperture VHF radar, *Icarus*, *188*, 162–174, 2007.
- Chau, J. L., I. Strelnikova, C. Schult, M. M. Oppenheim, M. C. Kelley, G. Stober, and W. Singer, Nonspecular meteor trails from non-field-aligned irregularities: Can they be explained by presence of charged meteor dust?, *Geophysical Research Letters*, *41*(10), 3336–3343, doi:10.1002/2014GL059922, 2014.
- Chau, J. L., G. Stober, C. M. Hall, M. Tsutsumi, F. I. Laskar, and P. Hoffmann, Polar mesospheric horizontal divergence and relative vorticity measurements using multiple specular meteor radars, *Radio Science*, *52*(7), 811–828, doi:10.1002/2016RS006225, 2016RS006225, 2017.
- Close, S., S. M. Hunt, M. J. Minardi, and F. M. McKeen, Analysis of Perseid meteor head echo data collected using the advanced research projects agency long-range tracking and instrumentation radar (ALTAIR), *Radio Science*, *35*(5), 1233–1240, doi:10.1029/1999RS002277, 2000.

Bibliography

- Close, S., S. M. Hunt, F. M. McKeen, and M. J. Minardi, Characterization of Leonid meteor head echo data collected using the VHF-UHF advanced research projects agency long-range tracking and instrumentation radar (ALTAIR), *Radio Science*, 37(1), 9–1–9–9, doi:10.1029/2000RS002602, 2002a.
- Close, S., M. Oppenheim, S. Hunt, and L. Dyrud, Scattering characteristics of high-resolution meteor head echoes detected at multiple frequencies, *Journal of Geophysical Research: Space Physics*, 107(A10), SIA 9–1–SIA 9–12, doi:10.1029/2002JA009253, 1295, 2002b.
- Close, S., M. Oppenheim, S. Hunt, and A. Coster, A technique for calculating meteor plasma density and meteoroid mass from radar head echo scattering, *Icarus*, 168, 43–52, 2004.
- Close, S., P. Brown, M. Campbell-Brown, M. Oppenheim, and P. Colestocka, Meteor head echo radar data: Mass-velocity selection effects, *Icarus*, 186, 547–556, 2007.
- Close, S., T. Hamlin, M. Oppenheim, L. Cox, and P. Colestock, Dependence of radar signal strength on frequency and aspect angle of nonspecular meteor trails, *Journal of Geophysical Research: Space Physics*, 113(A6), n/a–n/a, doi:10.1029/2007JA012647, a06203, 2008.
- de Oliveira-Costa, A., M. Tegmark, B. Gaensler, J. Jonas, T. Landecker, and P. Reich, A Model of Diffuse Galactic Radio Emission from 10 MHz to 100 GHz, *Mon. Not. R. Astron. Soc.*, 338, 247–260, 2008.
- Drolshagen, G., D. Koschny, S. Drolshagen, J. Kretschmer, and B. Poppe, Mass accumulation of earth from interplanetary dust, meteoroids, asteroids and comets, *Planetary and Space Science*, 143(Supplement C), 21 – 27, doi:https://doi.org/10.1016/j.pss.2016.12.010, sI:Meteoroids 2016, 2017.
- Dyrud, L. P., E. Kudeki, and M. Oppenheim, Modeling long duration meteor trails, *Journal of Geophysical Research: Space Physics*, 112(A12), –, doi:10.1029/2007JA012692, a12307, 2007.
- Fegley, B. J., and A. Cameron, A vaporization model for iron/silicate fractionation in the mercury protoplanet, *Earth and Planetary Science Letters*, 82, 207–222, 1987.
- Fentzke, J., D. Janches, and J. Sparks, Latitudinal and seasonal variability of the micrometeor input function: A study using model predictions and observations from Arecibo and PFISR, *Journal of Atmospheric and Solar-Terrestrial Physics*, 71, 653 – 661, advances in high latitude upper atmospheric science with the Poker Flat Incoherent Scatter Radar (PFISR), 2009.
- Fentzke, J. T., and D. Janches, A semi-empirical model of the contribution from sporadic meteoroid sources on the meteor input function in the mlt observed at arecibo, *Journal of Geophysical Research*, 113(A03304), 13 PP, 2008.
- Galligan, D. P., Structural analysis of radar meteoroid orbital data, Ph.D. thesis, University of Canderbury, 2000.

- Grün, E., M. Horanyi, and Z. Sternovsky, The lunar dust environment, *Planetary and Space Science*, 59(14), 1672 – 1680, doi:<https://doi.org/10.1016/j.pss.2011.04.005>, lunar Dust, Atmosphere and Plasma: The Next Steps, 2011.
- Grün, E., H. Zook, H. Fechtig, and R. Giese, Collisional balance of the meteoritic complex, *Icarus*, 62(2), 244 – 272, doi:[https://doi.org/10.1016/0019-1035\(85\)90121-6](https://doi.org/10.1016/0019-1035(85)90121-6), 1985.
- Haack, H., T. Grau, A. Bischoff, M. Horstmann, J. Wasson, A. Sorensen, M. Laubenstein, U. Ott, H. Palme, M. Gellissen, R. C. Greenwood, V. K. Pearson, I. A. Franchi, Z. Gabelica, and P. Schmitt-Kopplin, Maribo - A new CM fall from Denmark, *Meteoritics and Planetary Science* 47, 47, 30–50, doi:[doi:10.1111/j.1945-5100.2011.01311.x](https://doi.org/10.1111/j.1945-5100.2011.01311.x), 2012.
- Hey, J. S., S. J. Pasrsons, and G. S. Stewart, Radar Observations of the Giacobinid Meteor Shower, *Royal Astronomical Society*, 107, 176–183, 1947.
- Hill, K. A., L. A. Rogers, and R. L. Hawkes, Sputtering and high altitude meteors, *Earth, Moon, and Planets*, 95(1), 403–412, doi:[doi:10.1007/s11038-005-9018-x](https://doi.org/10.1007/s11038-005-9018-x), 2004.
- Hill, K. A., L. A. Rogers, and R. L. Hawkes, High geocentric velocity meteor ablation, *A&A*, 444(2), 615–624, doi:[doi:10.1051/0004-6361:20053053](https://doi.org/10.1051/0004-6361:20053053), 2005.
- Hocking, W., B. Fuller, and B. Vandepeer, Real-time determination of meteor-related parameters, *Journal of Atmospheric and Solar-Terrestrial Physics*, 63, 155–169, 2001.
- Janches, D., J. Mathews, D. Meisel, and Q.-H. Zhou, Micrometeor observations using the Arecibo 430 MHz radar: I. determination of the ballistic parameter from measured doppler velocity and deceleration results, *Icarus*, 145(1), 53 – 63, doi:<https://doi.org/10.1006/icar.1999.6330>, 2000.
- Janches, D., M. C. Nolan, D. D. Meisel, J. D. Mathews, Q. H. Zhou, and D. E. Moser⁵, On the geocentric micrometeor velocity distribution, *Journal of Geophysical Research*, 108, NO. A6, 1222, 2003.
- Janches, D., C. J. Heinselman, J. L. Chau, A. Chandran, and R. Woodman, Modeling the global micrometeor input function in the upper atmosphere observed by high power and large aperture radars, *Journal of Geophysical Research*, 111, A07,317, 2006.
- Janches, D., J. Hormaechea, C. Brunini, W. Hocking, and D. Fritts, An initial meteoroid stream survey in the southern hemisphere using the southern argentina agile meteor radar (SAAMER), *Icarus*, 223(2), 677 – 683, doi:<http://dx.doi.org/10.1016/j.icarus.2012.12.018>, 2013.
- Janches, D., W. Hocking, S. Pifko, J. L. Hormaechea, D. C. Fritts, C. Brunini, R. Michell, and M. Samara, Interferometric meteor head echo observations using the southern argentina agile meteor radar, *J. Geophys. Res. Space Physics*, 119, 2269–2287, 2014.

Bibliography

- Janches, D., N. Swarnalingam, J. D. Carrillo-Sanchez, J. C. Gomez-Martin, R. Marshall, D. Nesvorný, J. M. C. Plane, W. Feng, and P. Pokorný, Radar detectability studies of slow and small zodiacal dust cloud particles. III. the role of sodium and the head echo size on the probability of detection, *The Astrophysical Journal*, *843*(1), 1, 2017.
- Jenniskens, P., Meteor stream activity, *Astron. Astrophys.*, *287*, 990–1013, 1994.
- Jenniskens, P., *Meteor Showers and their Parent Comets*, 790 pp., Cambridge Univ Press, Cambridge, U.K., 2006.
- Jones, J., and P. Brown, Sporadic meteor radiant distributions: orbital survey results, *Mon. Not. R. Astron. Soc.*, *265*, 524–532, 1993.
- Jones, W., Theoretical and observational determinations of the ionization coefficient of meteors, *Monthly Notices of the Royal Astronomical Society*, *288*(4), 995–1003, doi:10.1093/mnras/288.4.995, 1997.
- Kelley, M. C., A new explanation for long-duration meteor radar echoes: Persistent charged dust trains, *Radio Science*, *39*(2), –, doi:10.1029/2003RS002988, rS2015, 2004.
- Kero, J., C. Szasz, A. Pellinen-Wannberg, G. Wannberg, A. Westman, and D. D. Meisel, Determination of meteoroid physical properties from tristatic radar observations, *Ann. Geophys.*, *26*, 2217–2228, 2008.
- Kero, J., C. Szasz, T. Nakamura, D. D. Meisel, M. Ueda, Y. Fujiwara, T. Terasawa, H. Miyamoto, and K. Nishimura, First results from the 2009-2010 MU radar head echo observation programme for sporadic and shower meteors: the Orionids 2009, *Mon. Not. R. Astron. Soc.*, *416*, 2550–2559, 2011.
- Kero, J., C. Szasz, T. Nakamura, T. Terasawa, H. Miyamoto, and K. Nishimura, A meteor head echo analysis algorithm for the lower VHF band, *Ann. Geophys.*, *30*, 639–659, 2012.
- Kero, J., C. Szasz, and T. Nakamura, MU head echo observations of the 2010 Geminids: radiant, orbit, and meteor flux observing biases, *Annales Geophysicae*, *31*(3), 439–449, doi:10.5194/angeo-31-439-2013, 2013.
- Latteck, R., W. Singer, M. Rapp, and T. Renkowitz, MAARSY - the new MST radar on Andoya/Norway, *Adv. Radio Sci.*, *8*, 1–6, 2010.
- Lau, E. M., S. K. Avery, J. P. Avery, D. Janches, S. E. P. R. Schafer, and N. A. Makarov, Statistical characterization of the meteor trail distribution at the South Pole as seen by a VHF interferometric meteor radar, *Radio Science*, *41*, 2006.
- Love, S. G., and D. E. Brownlee, A Direct Measurement of the Terrestrial Mass Accretion Rate of Cosmic Dust, *Science*, *262*(5133), 550–553, 1993.

- Low, F. J., D. A. Beintema, T. N. Gautier, F. C. Gillett, C. A. Beichman, G. Neugebauer, E. Young, H. H. Aumann, N. Boggess, J. P. Emerson, H. J. Habing, M. G. Hauser, J. R. Houck, M. Rowan-Robinson, B. T. Soifer, R. G. Walker, and P. R. Wesselius, Infrared cirrus: new components of the extended infrared emission, *The Astrophysical Journal*, 278, 19–22, 1984.
- Marshall, R. A., and S. Close, An FDTD model of scattering from meteor head plasma, *Journal of Geophysical Research: Space Physics*, 120(7), 5931–5942, doi:10.1002/2015JA021238, 2015JA021238, 2015.
- Marshall, R. A., P. Brown, and S. Close, Plasma distributions in meteor head echoes and implications for radar cross section interpretation, *Planetary and Space Science*, 143(Supplement C), 203 – 208, doi:https://doi.org/10.1016/j.pss.2016.12.011, sI:Meteoroids 2016, 2017.
- McKinley, D. W. R., *Meteor Science and Engineering*, McGraw-Hill, 1961.
- Michell, R., D. Janches, M. Samara, J. Hormaechea, C. Brunini, and I. Bibbo, Simultaneous optical and radar observations of meteor head-echoes utilizing saamer, *Planetary and Space Science*, 118(Supplement C), 95 – 101, doi:https://doi.org/10.1016/j.pss.2015.04.018, sI:ACM Interrelated, 2015.
- Moorhead, A. V., P. G. Brown, M. D. Campbell-Brown, D. Heynen, and W. J. Cooke, Fully correcting the meteor speed distribution for radar observing biases, *Planetary and Space Science*, 143(Supplement C), 209 – 217, doi:https://doi.org/10.1016/j.pss.2017.02.002, sI:Meteoroids 2016, 2017.
- Nesvorný, D., P. Jenniskens, H. F. Levison, W. F. Bottke, and D. Vokrouhlický, Cometary origin of the zodiacal cloud and carbonaceous micrometeorites; implications for hot debris disks, *The Astrophysical Journal*, 836, 713:816, 2010.
- Nesvorný, D., D. Vokrouhlický, P. Pokorný, and D. Janches, Dynamics of dust particles released from Oort cloud comets and their contribution to radar meteors, *The Astrophysical Journal*, 743(1), 37, 2011.
- Nishimura, K., T. Sato, T. Nakamura, and M. Ueda, High sensitivity radar-optical observations of faint meteors, *IEICE Transactions on Electronics*, E84-C, Issue 12, 1877–1884, 2001.
- Öpik, E. J., *Physics of Meteor Flight in the Atmosphere*, Interscience, London, 1958.
- Pellinen-Wannberg, A., A. Westman, G. Wannberg, and K. Kaila, Meteor fluxes and visual magnitudes from eiscat radar event rates: a comparison with cross-section based magnitude estimates and optical data, *Annales Geophysicae*, 16(11), 1475–1485, doi:10.1007/s00585-998-1475-x, 1998.
- Picone, J. M., A. E. Hedin, and D. P. Drob, NRLMSISE-00 empirical model of the atmosphere: Statistical comparisons and scientific issues, *Journal of Geophysical Research*, 107, 1468, 2002.

Bibliography

- Pifko, S., D. Janches, S. Close, J. Sparks, T. Nakamura, and D. Nesvorný, The meteoroid input function and predictions of mid-latitude meteor observations by the MU radar, *Icarus*, *223*, 444–459, 2013.
- Plane, J. M. C., Cosmic dust in the Earth’s atmosphere, *Chem. Soc. Rev.*, *41*, 6507–6518, doi:10.1039/C2CS35132C, 2012.
- Pokorný, P., D. Vokrouhlický, D. Nesvorný, M. Campbell-Brown, and P. Brown, Dynamical model for the toroidal sporadic meteors, *The Astrophysical Journal*, *789*(1), 25, 2014.
- Pokorný, P., D. Janches, P. Brown, and J. Hormaechea, An orbital meteoroid stream survey using the southern argentina agile meteor radar (SAAMER) based on a wavelet approach, *Icarus*, *290*(Supplement C), 162 – 182, doi:https://doi.org/10.1016/j.icarus.2017.02.025, 2017.
- Pokorný, P., and Brown, P. G., A reproducible method to determine the meteoroid mass index, *A&A*, *592*, A150, doi:10.1051/0004-6361/201628134, 2016.
- Renkowitz, T., W. Singer, R. Latteck, G. Stober, and M. Rapp, Validation of the radiation pattern of the Middle Atmosphere Alomar Radar System (MAARSY), *Adv. Radio Sci.*, *10*, 2012.
- Rogers, L., K. Hill, and R. Hawkes, Mass loss due to sputtering and thermal processes in meteoroid ablation, *Planetary and Space Science*, *53*(13), 1341–1354, doi:https://doi.org/10.1016/j.pss.2005.07.002, 2005.
- Schaefer, L., and B. Fegley, A thermodynamic model of high temperature lava vaporization on Io, *Icarus*, *169*, 216–241, 2004.
- Schult, C., G. Stober, J. L. Chau, and R. Latteck, Determination of meteor-head echo trajectories using the interferometric capabilities of MAARSY, *Ann. Geophys.*, *31*, 1843–1851, 2013.
- Schult, C., G. Stober, D. Keuer, and W. Singer, Radar observations of the Maribo fireball over Juliusruh: revised trajectory and meteoroid mass estimation, *MNRAS*, *450*, 1460–1464, 2015.
- Schult, C., G. Stober, D. Janches, and J. L. Chau, Results of the first continuous meteor head echo survey at polar latitudes, *Icarus*, *297*, 1–13, 2017.
- Schult, C., P. Brown, P. Pokorny, G. Stober, and J. L. Chau, A meteoroid stream survey using meteor head echo observations from the middle atmosphere alomar radar system (maarsy), *Icarus*, *submitted*, –, 2018.
- Silber, E. A., P. G. Brown, and Z. Krzeminski, Optical observations of meteors generating infrasound: Weak shock theory and validation, *Journal of Geophysical Research: Planets*, *120*(3), 413–428, doi:10.1002/2014JE004680, 2014JE004680, 2015.

- Stober, G., and J. L. Chau, A multistatic and multifrequency novel approach for specular meteor radars to improve wind measurements in the MLT region, *Radio Science*, *50*(5), 431–442, doi:10.1002/2014RS005591, 2014RS005591, 2015.
- Stober, G., C. Jacobi, and W. Singer, Meteoroid mass determination from underdense trails, *Journal of Atmospheric and Solar-Terrestrial Physics*, *73*, 895–900, 2011a.
- Stober, G., C. Jacobi, and W. Singer, Meteoroid mass determination from underdense trails, *Journal of Atmospheric and Solar-Terrestrial Physics*, *73*(9), 895 – 900, doi: <http://dx.doi.org/10.1016/j.jastp.2010.06.009>, scientific Results from Networked and Multi-instrument studies based on MST Radar, 2011b.
- Stober, G., C. Jacobi, V. Matthias, P. Hoffmann, and M. Gerding, Neutral air density variations during strong planetary wave activity in the mesopause region derived from meteor radar observations, *Journal of Atmospheric and Solar-Terrestrial Physics*, *74*, 55 – 63, 2012.
- Stober, G., V. Matthias, P. Brown, and J. L. Chau, Neutral density variation from specular meteor echo observations spanning one solar cycle, *Geophys. Res. Lett.*, *41*, 6919–6925, 2014.
- Taylor, A. D., Radiant distribution of meteoroids encountering the earth, *Adv. Space Res.*, *20*, 1505–1508, 1997.
- Thomas, E., M. Horányi, D. Janches, T. Munsat, J. Simolka, and Z. Sternovsky, Measurements of the ionization coefficient of simulated iron micrometeoroids, *Geophysical Research Letters*, *43*(8), 3645–3652, doi:10.1002/2016GL068854, 2016GL068854, 2016.
- Tielens, A. G. G. M., C. F. McKee, C. G. Seab, and D. J. Hollenbach, The physics of grain-grain collisions and gas-grain sputtering in interstellar shocks, *ApJ*, *431*, 321–340, doi:10.1086/174488, 1994.
- Verniani, F., An analysis of the physical parameters of 5759 faint radio meteors, *Journal of Geophysical Research*, *78*(35), 8429–8462, doi:10.1029/JB078i035p08429, 1973.
- Vondrak, T., J. M. C. Plane, S. Broadley, and D. Janches, A chemical model of meteoric ablation, *Atmos. Chem. Phys.*, *8*, 7015–7031, 2008.
- Weryk, R., M. Campbell-Brown, P. Wiegert, P. Brown, Z. Krzeminski, and R. Musci, The canadian automated meteor observatory (CAMO): System overview, *Icarus*, *225*(1), 614 – 622, doi:<https://doi.org/10.1016/j.icarus.2013.04.025>, 2013.
- Weryk, R. J., and P. G. Brown, Simultaneous radar and video meteors -II: Photometry and ionisation, *Planetary and Space Science*, *81*(Supplement C), 32 – 47, doi:<https://doi.org/10.1016/j.pss.2013.03.012>, 2013.
- Whipple, F. L., 1983 TB and the Geminid Meteors, *IAU Circ.*, *3881*, 1983.
- Wiegert, P., and P. Brown, The quadrantid meteoroid complex, *Icarus*, *179*(1), 139 – 157, doi:<https://doi.org/10.1016/j.icarus.2005.05.019>, 2005.

Bibliography

- Wiegert, P., J. Vaubaillon, and M. Campbell-Brown, A dynamical model of the sporadic meteoroid complex, *Icarus*, *201* (1), 295 – 310, doi:<https://doi.org/10.1016/j.icarus.2008.12.030>, 2009.
- Williams, E. R., Y.-J. Wu, J. Chau, and R.-R. Hsu, Intercomparison of radar meteor velocity corrections using different ionization coefficients, *Geophysical Research Letters*, *44* (11), 5766–5773, doi:10.1002/2017GL073610, 2017GL073610, 2017.
- Williams, I., and Z. Wu, The Geminid meteor stream and asteroid 3200 Phaethon, *Monthly Notices of the Royal Astronomical Society*, *262*, no. 1, 231–248, 1993.

Appendix A Schult et al. (2013)

C. Schult , G. Stober, J. L. Chau and R. Latteck, Determination of meteor-head echo trajectories using the interferometric capabilities of MAARSY, *Ann. Geophys.*, **31**, 1843-1851, 2013, doi:10.5194/angeo-31-1843-2013.

Appendix B Schult et al. (2015)

C. Schult, G. Stober, D. Keuer and W. Singer, Radar observations of the Maribo fireball over Juliusruh: revised trajectory and meteoroid mass estimation, MNRAS 450, 1460–1464, 2015, doi:10.1093/mnras/stv614.

Appendix C Schult et al. (2017)

C. Schult, G. Stober, D. Janches, J. L. Chau, Results of the first continuous meteor head echo survey at polar latitudes, *Icarus*, 297, 1-13, 2017.
<http://dx.doi.org/10.1016/j.icarus.2017.06.019>

Appendix D Brown et al. (2017)

P. Brown, G. Stober, C. Schult, Z. Krzeminski, W. Cooke, J.L. Chau, Simultaneous optical and meteor head echo measurements using the Middle Atmosphere Alomar Radar System (MAARSY): Data collection and preliminary analysis, Planetary and Space Science, 141, 25-34, 2017, 10.1016/j.pss.2017.04.013.

Appendix E Schult et al. (2018)

C. Schult, P. Brown, P. Pokorný, G. Stober, J. L. Chau, A meteoroid stream survey using meteor head echo observations from the Middle Atmosphere ALOMAR Radar System (MAARSY), *Icarus*, 309, 177-186, 2018. <https://doi.org/10.1016/j.icarus.2018.02.032>

Appendix F Meteor head echo data analysis

The radar raw data consists of a matrix with complex voltages ($raw = ip + i \cdot qp$, in-phase (ip) and quadrature phase (qp)) in three dimensions (range gates, consecutive pulses, receiver channels). At the first step the direct current is removed by subtracting the median values for qp and ip for each receiving channel separately. Afterwards a phase correction for every receiving channel is applied. The corresponding phases $\Delta\phi$ are calculated by using radio sources as shown in *Chau et al. (2014)*. The phase correction is also added to every receiver channel separately: $raw \cdot e^{-i\Delta\phi}$

The next step is the decoding of the raw data considering the Doppler velocity of the meteor head echo. Transmitted radar pulses are often modified with phase codes, which make it possible to increase the signal to noise ratio. The experiment mode used in *Schult et al. (2017)* and *Brown et al. (2017)* is configured to observe multiple mesospheric targets at the same time, what makes it in the case of volume scatterers (such as polar mesospheric summer echoes, PMSE) necessary to use complementary codes. The side lobes of two consecutive complementary codes cancel each other by summing up the decoded code pairs. In the case of meteor head echoes, which have very high Doppler velocities and fast range gate transitions, it is necessary to keep both codes separated and to do the Doppler decoding for each head echo individually. The code pairs in the experiment are defined as:

$$\begin{aligned} C_1 &= [1, -1, -1, -1, 1, 1, -1, 1, 1, -1, -1, -1, -1, 1, -1] \\ C_2 &= [-1, 1, -1, -1, -1, -1, -1, -1, 1, -1, 1, -1, -1, 1, 1] \end{aligned} \quad (F.1)$$

, where -1 and 1 indicate 180° phase shifts in the complex notation. For the usage of a fast Fourier transformation (FFT) the code vectors are refilled with zeros to the length of the range gate numbers (first dimension of raw). The Doppler frequency of a target is calculated using:

$$f_D = 2f_0 v_r / c \quad (F.2)$$

with f_D the Doppler frequency, the f_0 radar frequency, v_r radial velocity of the target and c the speed of light. The target shifts, due to the line-of-sight velocity (v_r), the transmitted pulse and the initialized code has to be adapted to fit the received one by considering the Doppler frequency (*Kero et al., 2012*):

$$C_{1D} = C_1 e^{-i2\pi f_D T_s k} \quad (F.3)$$

with $k = 0, 1, 2 \dots 15$ (code length) and T_s the sampling time. The raw data is then decoded with the Doppler corrected phase codes C_{1D} and C_{2D} using a convolution:

$$raw_{dec} = ifft(fft(raw) \cdot fft(C_{1D})^*) \quad (F.4)$$

with $ifft$ the inverse fast Fourier transformation. To find the correct Doppler frequency, an iterative method is used with a maximum velocity resolution of $\Delta v_r = 0.1$ km/s. The maximum amplitude of the decoded pulse has to be five times larger than the median background noise to be accepted as a head echo signal. This procedure is done for every pulse, considering significant deceleration during the time of detection. After the raw matrix for the first receiver is decoded, the same velocity values are used for the decoding of the other receiving channels.

The decoded raw data matrix raw_{dec} is now used for the further analysis. At first, the signal to noise ratio (SNR) is calculated:

$$\begin{aligned} P &= |raw_{dec}|^2 \\ S &= P - N \\ SNR &= 10\log_{10}(S) - 10\log_{10}(N) - 10\log_{10}(16) \end{aligned} \quad (F.5)$$

with the voltage power P , signal power S and noise power N . The noise power is determined by the median value of the voltage of range gates where probably no signal is observed. The value of 16 is subtracted due to the additional SNR of the phase code.

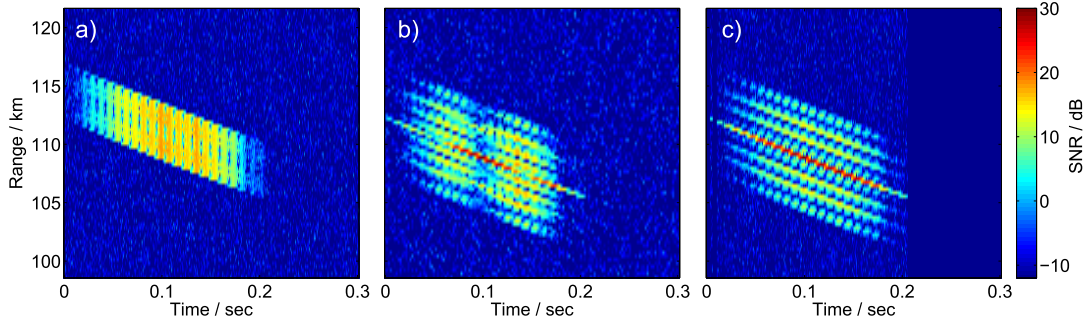


Figure F.1 SNR (of receiving channel one) versus range and time of the same meteor head echo for different decoded signals: a) undecoded signal (raw); b) decoded without considering the Doppler velocity; c) Doppler decoded signal (raw_{dec}).

For each time step (received pulse) the voltage of the range gate with the highest SNR is used for the interferometric analysis. The phase differences between different receiving channels (e.g., raw_{dec_1} and raw_{dec_2})

$$\Delta\Phi = \angle raw_{dec_1} raw_{dec_2}^* = \arctan\left(\frac{Re(raw_{dec_1} raw_{dec_2}^*)}{Im(raw_{dec_1} raw_{dec_2}^*)}\right) \quad (F.6)$$

can be used to calculate the location of the meteor head within the radar beam. The SNR within one receiving channel as well as the distance (baseline) between two receivers affect the accuracy of the interferometric position. Due to the 2π periodicity of the phase differences, an ambiguity area for the position solution is defined. Larger baselines have higher accuracy but a smaller ambiguity area, while smaller baselines

Appendix F Meteor head echo data analysis

result in a lower accuracy with a larger ambiguity area. To combine the advantages of small and long baselines, the target position is calculated in two steps. At first, the receiving channels with the smallest distances (e.g. receiver constellation B06, B08 and C02 in Figure 1 in (Schult *et al.*, 2017)) were used to calculate a mean direction for the integrated head echo signal. The set of equations for smaller baselines ($\Delta\Phi_{S_1} \dots \Delta\Phi_{S_N}$ with N the number of receiver pairs) is then solved with a least squares method (e.g., Lau *et al.*, 2006):

$$\begin{pmatrix} \Delta\Phi_{S_1} \\ \vdots \\ \Delta\Phi_{S_N} \end{pmatrix} = -\frac{2\pi}{\lambda} \begin{pmatrix} d_{S_1} \cos(\gamma_{S_1}) & d_{S_1} \sin(\gamma_{S_1}) \\ \vdots & \vdots \\ d_{S_N} \cos(\gamma_{S_N}) & d_{S_N} \sin(\gamma_{S_N}) \end{pmatrix} \cdot \begin{pmatrix} \cos(\alpha) \cos(\beta) \\ \cos(\alpha) \sin(\beta) \end{pmatrix}, \quad (\text{F.7})$$

with the radar wavelength λ , the receiver distances d and angles γ and the target azimuth and zenith angles β and α . Afterwards, the solution of the small baseline antenna configuration is used to calculate the natural numbers $n_1 \dots n_N$ (for every receiver pair), which has to be added to the phase differences of the large baseline configuration:

$$\begin{pmatrix} \Delta\Phi_{L_1} + 2n_1\pi \\ \vdots \\ \Delta\Phi_{L_N} + 2n_N\pi \end{pmatrix} = -\frac{2\pi}{\lambda} \begin{pmatrix} d_{L_1} \cos(\gamma_{L_1}) & d_{L_1} \sin(\gamma_{L_1}) \\ \vdots & \vdots \\ d_{L_N} \cos(\gamma_{L_N}) & d_{L_N} \sin(\gamma_{L_N}) \end{pmatrix} \cdot \begin{pmatrix} \cos(\alpha) \cos(\beta) \\ \cos(\alpha) \sin(\beta) \end{pmatrix}. \quad (\text{F.8})$$

For the larger baselines the set of equations is solved for every single pulse to get the angular evolution of the target motion within the radar beam. In combination with the target range information (range gate with the highest SNR) and the time ($\Delta t = 1/PRF$) between consecutive pulses, the three dimensional trajectory is obtained. The spherical coordinates ($range, \alpha, \beta$) are transformed into cartesian coordinates (x, y, z) and fitted over the time (t) to obtain the meteor head mean velocity and entry angle.

A more precise meteor velocity and the deceleration is calculated out of the pulse-to-pulse phase correlation (e.g., Chau and Woodman, 2004; Kero *et al.*, 2012):

$$v_r = -\frac{\Delta\Phi}{\Delta t} \frac{\lambda}{4\pi}, \quad (\text{F.9})$$

in this case, $\Delta\Phi$ represents the phase difference between consecutive received pulses of a single receiver (receiving channel one due to the highest SNR). Again, $\Delta\Phi$ has multiple solutions of $2n\pi$ due to the large meteor velocities. The natural number n is calculated using the mean velocity of the interferometric trajectory solution. To obtain the absolute velocity, for every time step, the radial velocity v_r has to be corrected for the angle (ω) between meteor trajectory (entry elevation (ele) and azimuth (azi)) and the radial component (α, β):

$$\begin{aligned} \cos(\omega) &= \begin{pmatrix} \cos(\alpha) \sin(\beta) \\ \cos(\alpha) \cos(\beta) \\ \sin(\alpha) \end{pmatrix} \cdot \begin{pmatrix} \cos(ele) \sin(azi) \\ \cos(ele) \cos(azi) \\ \sin(ele) \end{pmatrix} \\ v_{abs} &= \frac{v_r}{\cos(\omega)} \end{aligned} \quad (\text{F.10})$$

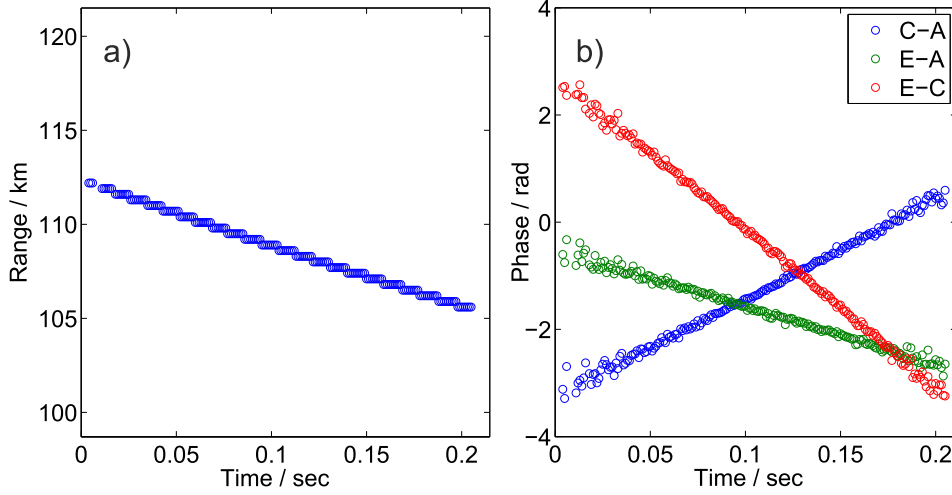


Figure F.2 a) range versus time (range gates with the highest SNR); b) phase differences between three large baseline receiver constellations ($\Delta\Phi_{L_1}, \Delta\Phi_{L_2}, \Delta\Phi_{L_3}$ in equation F.8).

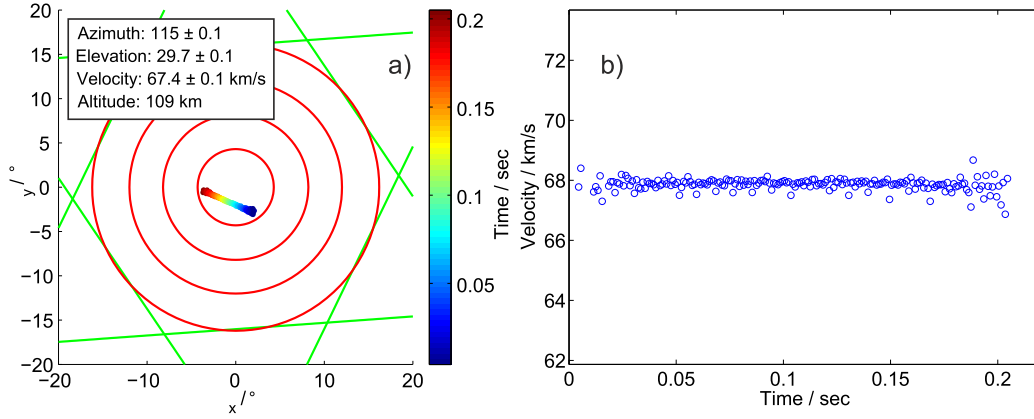


Figure F.3 a) trajectory solution of the meteor head echo; red circles indicate minima of the MAARSY radiation pattern and green lines show the ambiguity area; the fitted entry angle and velocity is shown in the legend. Note that $\Theta_x = \cos(\alpha) \cos(\beta)$ and $\Theta_y = \cos(\alpha) \sin(\beta)$; b) velocity versus time from the pulse to pulse analysis (v_{abs} in equation F.10).

The last parameter which is calculated directly from the raw data is the radar cross section (σ). In the case of meteor head echoes, which are not beam filling targets, the hard target equation is used (*Close et al.*, 2002b; *Kero et al.*, 2012):

$$\sigma = \frac{(4\pi)^3 R^4 P_R}{G_T G_R \lambda P_T} \quad (\text{F.11})$$

Appendix F Meteor head echo data analysis

with R the range of the head echo, P_R the received power, G_T, G_R the antenna gain for transmission and reception and P_T the transmitted power. The transmitted power can be calculated with the number of transmitting antennas (433) and the corresponding power for each transceiver module (2000W). In addition some corrections have to be included, due to the fact that not the whole power of the modules is transmitted through the antenna (factor 0.85) and that some transceiver could be damaged (n_d):

$$P_T = (433 - n_d) \cdot 2000W \cdot 0.85 \quad (\text{F.12})$$

The received power is determined from the signal SNR, the background noise T_N and the bandwidth ($b_w = 500\text{kHz}$):

$$\begin{aligned} P_R &= \text{SNR} \cdot T_N k_B b_w \\ T_N &= T_{sys} + T_{sky} \end{aligned} \quad (\text{F.13})$$

with k_B the Boltzmann constant. The background noise temperature is a combination of the system noise temperature ($T_{sys} = 800\text{K}$) and the sky noise temperature ($T_{sky} = 3300\text{K}$ up to 7700K). T_{sky} is determined by a convolution of the MAARSY gain pattern and the sky noise model from *de Oliveira-Costa et al. (2008)* (see also *Stober et al. (2011b)*; *Renkowitz et al. (2012)* and Figure F.4). Figure F.4 b) to c) show the SNR , antenna gain and RCS of the meteor head echo for the trajectory shown in Figure F.3 a). Note that the SNR drops down for several dB during the transition between the range gate. The drop in the SNR is a measurement artifact, which is removed in Figure F.4 with an interpolation between the maxima.

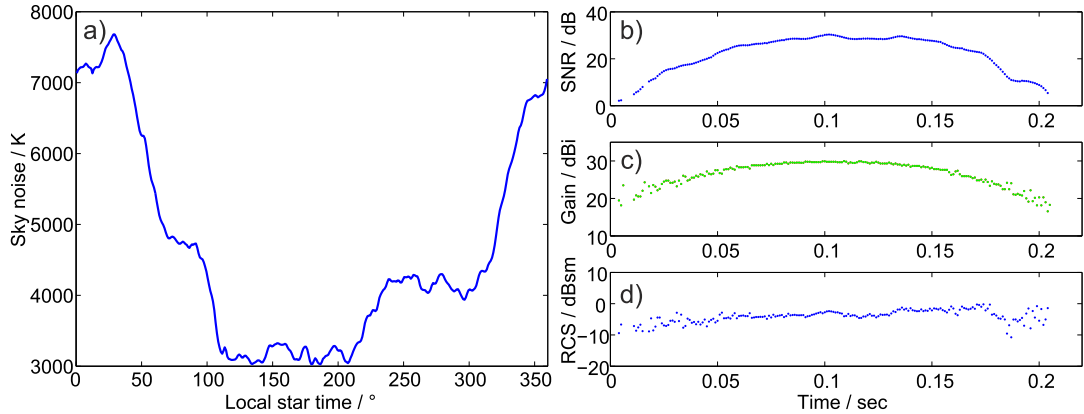


Figure F.4 a) Sky noise temperature (T_{sky}) of MAARSY for different local star times. b) SNR versus time of the meteor head echo. c) MAARSY antenna gain for the different positions of the head echo in the radar beam. d) Radar cross section (RCS or σ) of the meteor head echo.

Acknowledgements

I would like to thank my first Advisor and head of the radar department, Prof. Dr. Jorge L. Chau, for supervising my thesis and for giving me the opportunity to work in his department. His ideas, advices and his encouragement on the daily meteor head echo observation helped me a lot for my thesis. Furthermore, my special thanks goes to my second advisor Dr. Gunter Stober, for funding my research through the AHEAD project (grant STO 1053/1-1 (AHEAD) of the Deutsche Forschungsgemeinschaft). I had a great time during our trips to a variety of conferences and workshops. I would like to thank Diego Janches for the cooperation and the great time during my stay at the Goddard Space Flight Center. Also the cooperation with Peter Brown was a great pleasure for me. We had great discussion during the several stays at the University of Western Ontario. I also want to thank my great colleagues, Svenja Sommer, Sven Wilhelm, Heiner Asmus and Vivien Matthias. It were not primarily the science related discussions with you, which made the time in the office much more joyful. At the end I want to thank the technical staff of the radar department of the IAP. Without the work of Ralph Latteck, Marius Zecha, Jörg Trautner, Thomas Barth and Jens Wedrich, the wonderful radar system MAARSY would not exist and no meteor head echo data could have been analyzed.

Curriculum Vitae

Personal Data

- Name: Schult, Carsten
- Date of Birth: 06.07.1987
- Place of Birth: Rostock

Scientific career

- since 12/2012 PhD student at the Leibniz-Institut of Atmospheric Physics at the University of Rostock, Advisor: Prof. Jorge L. Chau
- 10/2010-10/2012 Master of Science in Physics, University of Rostock
Master thesis: Bestimmung von Trajektorien von Meteor-Kopf-Echos mittels Interferometrie (Trajectory-determination of meteor head echoes using radar interferometry), Advisor: Prof. Markus Rapp
- 10/2007-09/2010 Bachelor of Science in Physics, University of Rostock
Bachelor thesis: Entstehungsszenarien großer Planeten (Processes of Planet Formation), Advisor: Prof. Dr. Ronald Redmer
- 07/2006 Abitur, Goethe Gymnasium Rostock

List of Publications

- G. Stober, C. Schult, C. Baumann, R. Latteck and M. Rapp, The Geminid meteor shower during the ECOMA sounding rocket campaign: specular and head echo radar observations, *Ann. Geophys.*, 31, 473-487, 2013, doi:10.5194/angeo-31-473-2013.
- S. Sommer, G. Stober, C. Schult and R. Latteck, Investigation of horizontal structures at mesospheric altitudes using coherent radar imaging, *Adv. Radio Sci.*, 11, 319-325, 2013, doi:10.5194/ars-11-319-2013.

- C. Schult , G. Stober, J. L. Chau and R. Latteck, Determination of meteor-head echo trajectories using the interferometric capabilities of MAARSY, *Ann. Geophys.*, 31, 1843-1851, 2013, doi:10.5194/angeo-31-1843-2013.
- J. L. Chau, I. Strelnikova, C. Schult, M. M. Oppenheim, M. C. Kelley, G. Stober and W. Singer, Nonspecular meteor trails from non-field-aligned irregularities: Can they be explained by presence of charged meteor dust?, *Geophys. Res. Lett.*, 41 3336-3343, doi:10.1002/2014GL 059922.
- T. Renkwitz, C. Schult, R. Latteck and G. Stober, Validation of the radiation pattern of the VHF MST radar MAARSY by scattering off a sounding rocket's payload, *Adv. Radio Sci.*, 13, 41-48, 2015, doi:10.5194/ars-13-41-2015.
- C. Schult, G. Stober, D. Keuer and W. Singer, Radar observations of the Maribo fireball over Juliusruh: revised trajectory and meteoroid mass estimation, *MNRAS* 450, 1460-1464, 2015, doi:10.1093/mnras /stv614.
- S. Sommer, J. L. Chau, and Carsten Schult, On high time-range resolution observations of PMSE: Statistical characteristics, *J. Geophys. Res. Atmos.*, 121, 6713-6722, doi:10.1002/2015JD024531.
- T. Renkwitz, C. Schult and Ralph Latteck, VHF antenna pattern characterization by the observation of meteor head echoes, *Atmos. Meas. Tech.*, 10, 527-535, 2017, doi:10.5194/amt-10-527-2017.
- P. Brown, G. Stober, C. Schult, Z. Krzeminski, W. Cooke, J.L. Chau, Simultaneous optical and meteor head echo measurements using the Middle Atmosphere Alomar Radar System (MAARSY): Data collection and preliminary analysis, *Planetary and Space Science*, 141, 25-34, 2017, 10.1016/j.pss.2017.04.013.
- C. Schult, G. Stober, D. Janches, J. L. Chau, Results of the first continuous meteor head echo survey at polar latitudes, *Icarus*, 297, 1-13, 2017. <http://dx.doi.org/10.1016/j.icarus.2017.06.019>

Erklärung über den Eigenanteil an den Manuskripten

Diese kumulative Dissertation ist eine Zusammenfassung aus insgesamt fünf Veröffentlichungen, wobei Herr Schult bei vier Veröffentlichungen Erstautor und bei einer weiteren Arbeit Co-Autor ist. Im Folgenden wird der Arbeitsanteil von Herrn Schult an den Veröffentlichungen aufgezeigt.

In Schult et al. 2013 wurden das erste Mal Meteorkopfechomessungen mit dem Radarsystem MAARSY durchgeführt. Die Idee dieser Messungen stammt von Dr. Stober und die Experimentdaten waren bereits verfügbar. Die Rohdatenanalyse, bis hin zur graphischen Darstellung (Ausnahme Bild 10), wurde durch Herrn Schult durchgeführt. Der Text wurde ebenfalls von Herrn Schult verfasst. Der Anteil der Co-Autoren liegt bei der Experiment Erstellung/Umsetzung und bei der Diskussion und Überarbeitung des Manuskriptes.

In Schult et al. 2015 wurde die Trajektorie des Maribo Feuerballs untersucht und eine Massenabschätzung mithilfe eines Ablationsmodelles vorgenommen. Die Rohdatenanalyse und die Trajektorienbestimmung erfolgte durch Herrn Schult. Das verwendete Ablationsmodell wurde durch Dr. Stober entwickelt und an die vorher bestimmten Parameter angepasst. Die erhaltenen Kurven wurden gemeinsam diskutiert und ausgewertet. Der Text und die Graphiken wurden von Herrn Schult erstellt.

In Schult et al. 2017 werden die ersten quasi-kontinuierlichen Meteorkopfechomessungen mit dem Radarsystem MAARSY vorgestellt. Die Idee für ein gemeinsames Messexperiment stammt von Prof. J. L. Chau. Das benötigte Experimentdesign, in Bezug auf die Meteorbeobachtungen, wurde von Herrn Schult erarbeitet. Auch die Rohdatenanalyse bis hin zur graphischen Darstellung erfolgte durch Herrn Schult. Hierbei werden die Meteordaten getrennt von der Standardanalyse behandelt. Das Modell für den Meteoreintrag wurde durch D. Janches zur Verfügung gestellt und durch Herrn Schult an die MAARSY-Parameter angepasst. Anschließend erfolgte eine gemeinsame Auswertung und Diskussion. Text und Graphiken in dem Manuskript stammen von Herrn Schult.

In Brown et al. 2017 werden Vergleichsmessungen der MAARSY Meteorkopfechomessungen mit optischen Kamerasystemen vorgestellt. Dieses Manuskript entstand durch eine Kooperation mit der University of Western Ontario und der NASA. Die Installation der Kamerasysteme und die optische Auswertung, wurde durch die externen Partner realisiert. Dabei wurden MAARSY Daten zur anfänglichen Justierung der Systeme herangezogen. Die Auswertung und manuelle Qualitätsprüfung der einzelnen Meteorkopfechos in den Radardaten wurde durch Herrn Schult erarbeitet. In mehreren Treffen wurden die gleichzeitigen Messungen gemeinsam überprüft und ausgewertet. Text und finale Graphiken wurden hauptsächlich durch den Erstautor P. Brown erstellt.

Schult et al. 2018 beinhaltet die Auswertung der Meteorkopfechodaten von MAARSY in Bezug auf beobachtete Meteorschauer. Die Arbeit ist in enger Zusammenarbeit mit der University of Western Ontario (Peter Brown) und Petr Pokorný entstanden. Die Wavelet-Meteorschauer-Software ist ein fertiges Softwaretool, wobei die MAARSY-Daten für die Analyse von Herrn Schult entsprechend aufbereitet wurden. Die manuelle Auswertung der Wavelet Daten erfolgte durch alle Autoren und wurde anschließend gemeinsam diskutiert. Die Schauer Indizes wurden mithilfe des Multi-Nest Algorithmus von Petr Pokorný durchgeführt. Die vorherige Datenfilterung und eine unabhängige manuelle Berechnung zur Kontrolle erfolgte durch Herrn Schult. Text und Bilder des Manuskriptes wurden größtenteils durch Herrn Schult erstellt und anschließend mithilfe der Co-Autoren diskutiert und überarbeitet.

Selbstständigkeitserklärung

Hiermit versichere ich an Eides statt, die vorgelegte Arbeit selbstständig und ohne fremde Hilfe verfasst, keine außer den von mir angegebenen Hilfsmitteln und Quellen dazu verwendet und die den benutzten Werken inhaltlich und wörtlich entnommenen Stellen als solche kenntlich gemacht zu haben.

Die Arbeit wurde bisher weder im Inland noch im Ausland in gleicher oder ähnlicher Form einer anderen Prüfungsbehörde vorgelegt. Weiterhin erkläre ich, dass ich ein Verfahren zur Erlangung des Doktorgrades an keiner anderen wissenschaftlichen Einrichtung beantragt habe.

Kühlungsborn, den 16. Februar 2018

(Carsten Schult)

,